

# Numerical Modeling of Weather and Climate

Christoph Schär, Institute for Atmospheric and Climate Science ETH, 8092 Zürich  
<http://www.iac.ethz.ch/people/schaer>

## Chapter 3: Adiabatic Formulation of Atmospheric Models

March 2015

<b>3.1 Shallow water dynamics .....</b>	<b>3.3</b>
3.1.1 Background .....	3.3
3.1.2 Linearization and wave propagation .....	3.4
3.1.3 Integration in advective form using centered differences .....	3.5
3.1.4 Integration in flux form using the Euler time step .....	3.6
<b>3.2 Quasi-geostrophic dynamics.....</b>	<b>3.9</b>
<b>3.3 Coordinate transformation.....</b>	<b>3.11</b>
3.3.1 Motivation .....	3.11
3.3.2 Wind vector and advection operator in generalized coordinates	3.13
3.3.3 Transformation of derivatives with generalized coordinates .....	3.14
3.3.4 Transformation of the horizontal momentum equation.....	3.15
<b>3.4 Hydrostatic dynamics in pressure coordinates.....</b>	<b>3.18</b>
<b>3.5 Isentropic coordinates.....</b>	<b>3.20</b>
3.5.1 Background .....	3.20
3.5.2 Isentropic form of governing equations .....	3.21
3.5.3 Numerical integration.....	3.24
<b>3.6 Sigma coordinates .....</b>	<b>3.28</b>
3.6.1 Transformation of hydrostatic equations in $\sigma$ -coordinates .....	3.28
3.6.2 Summary of equations and boundary conditions .....	3.29
3.6.3 Numerical integration.....	3.31
3.6.4 Additional aspects of terrain-following coordinates .....	3.33
<b>3.7 Spectral methods .....</b>	<b>3.35</b>
3.7.1 Classical spectral methods .....	3.35
3.7.2 Pseudo-spectral method .....	3.38
3.7.3 Global spectral models .....	3.39
<b>3.8 References .....</b>	<b>3.42</b>



### 3. Adiabatic formulation of atmospheric models

#### 3.1 Shallow water dynamics

##### 3.1.1 Background

The shallow water equations represent the simplest model problem for stratified fluids (a fluid with vertically decreasing density). The system of equations is employed in atmospheric and oceanic sciences to investigate elementary properties of stratified fluid dynamics.

The shallow water equations represent the dynamics of a homogeneous layer of incompressible fluid of constant density, which is confined above by a free surface. The free surface represents a discontinuous density interface, and it implies stratification effects. The one-dimensional shallow-water system is sketched in Fig.3.1.1. We make two important assumptions: First, the interaction with the overlying layer of fluid (e.g. air) is neglected. Second, it is assumed that the horizontal velocity is independent of height, i.e.  $\partial u / \partial z = 0$ . The latter assumption restricts the validity of the system to shallow fluid layers.

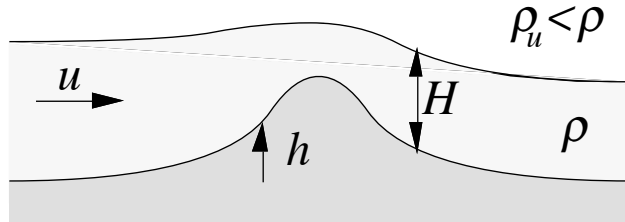


**Fig.3.1.1:** Variables in the one-dimensional shallow water equations:  
horizontal velocity  $u$ , layer depth  $H$ , height of topography  $h$ .

In the one-dimensional case and in the absence of background rotation, the shallow-water equations encompass a horizontal momentum equation

$$\frac{Du}{Dt} + g^* \frac{\partial(h+H)}{\partial x} = 0 \quad \text{with} \quad \frac{D}{Dt} = \frac{\partial}{\partial t} + u \frac{\partial}{\partial x}, \quad (3.1.1)$$

and a continuity equation

$$\frac{\partial H}{\partial t} + \frac{\partial(uH)}{\partial x} = 0. \quad (3.1.2)$$

Here  $g^* = g\Delta\rho/\rho$  with  $\Delta\rho = \rho - \rho_u$  denotes the reduced gravity. For a lake or river (where  $\rho$  and  $\rho_u$  represent water and air, respectively), we have  $g^* \approx g$ . However, the shallow water equations may be used to represent a wide range of other two-layer systems. For instance, an atmospheric two-layer structure may be represented as  $g^* = g\Delta\theta/\theta$ , where  $\Delta\theta$  denotes the potential temperature contrast across the interface between the two layers.

The shallow water equations support propagating shallow-water waves. In the approximation considered, they are non-dispersive and have phase (and group) velocities given by

$$c = \sqrt{g^* H} \quad (3.1.3)$$

An associated non-dimensional parameter is the *Froude number*

$$Fr = \frac{|u|}{\sqrt{g^* H}}, \quad (3.1.4)$$

which is defined as the ratio between advective and phase velocities. The Froude number is used to distinguish between two major flow regimes. Flows with  $Fr < 1$  are referred to as *subcritical*. In these flows, the group velocity exceeds the advective velocity. Thus, waves are able to propagate against the mean flow. Flows with  $Fr > 1$  are referred to as *supercritical*. In supercritical flow, upstream propagating waves are flushed downstream by the advective velocity. Thus, there is a kind of communication problem, in the sense that the presence of an obstacle in a supercritical flow cannot be communicated into the upstream direction. Supercritical flows can thus lead to the formation of a *hydraulic jump* (or *shock*). In analytical theory, these are discontinuities in layer depth and flow velocity. Examples of such features in the shallow water systems include hydraulic jumps in rivers and kitchen sinks (kayak sportsmen and cooks should know about these!). Related phenomena occur in supersonic booms (aviation), foehn winds and downslope windstorms (meteorology), or traffic jams (transportation). In all these examples, the key issue is the inability of wave propagation against the mean flow.

### 3.1.2 Linearization and wave propagation

This subsection provides additional details regarding the wave propagation in the shallow water system. The derivation of (3.1.3) is based on a linearization of the system in absence of topography. To this end, the flow variables are expanded as

$$u(x,t) = \bar{u} + u'(x,t) \quad \text{and} \quad H(x,t) = \bar{H} + H'(x,t)$$

where the base state  $\bar{u}$ ,  $\bar{H}$  is a time-independent (trivial) solution of the governing equations. Equations (3.1.1-2) can then be expressed as

$$\begin{aligned} \frac{\partial u'}{\partial t} + (\bar{u} + u') \frac{\partial u'}{\partial x} + g^* \frac{\partial H'}{\partial x} &= 0, \\ \frac{\partial H'}{\partial t} + (\bar{u} + u') \frac{\partial H'}{\partial x} + \frac{\partial u'}{\partial x}(\bar{H} + H') &= 0. \end{aligned}$$

The linearization involves dropping all nonlinear terms. In the quiescent case  $\bar{u} = 0$  this yields

$$\begin{aligned} \frac{\partial u'}{\partial t} + g^* \frac{\partial H'}{\partial x} &= 0, \\ \frac{\partial H'}{\partial t} + \frac{\partial u'}{\partial x} \bar{H} &= 0. \end{aligned}$$

With the complex wave-Ansatz

$$u' = \tilde{u} e^{i(kx-\omega t)} \quad \text{and} \quad H' = \tilde{H} e^{i(kx-\omega t)} \quad (\text{with wave amplitudes } \tilde{u} \text{ and } \tilde{H})$$

the linearized system yields

$$-i\omega \tilde{u} + ik g^* \tilde{H} = 0 ,$$

$$-i\omega \tilde{H} + ik \tilde{u} \bar{H} = 0 ,$$

where we have divided by  $e^{i(kx-\omega t)}$ . Elimination of  $\tilde{H}$  and solving for  $\omega$  yields the dispersion relation

$$\omega^2 = g^* \bar{H} k^2 \quad \text{or} \quad \omega = \pm \sqrt{g^* \bar{H}} k$$

This is a non-dispersive system, i.e. phase and group velocities are identical and given by

$$u_p = \frac{\omega}{k} = \pm \sqrt{g^* \bar{H}} \quad \text{and} \quad c_p = \frac{\partial \omega}{\partial k} = \pm \sqrt{g^* \bar{H}} .$$

Waves may propagate in both direction and their velocity is independent of the wave length  $k$ .

### 3.1.3 Integration in advective form using centered differences

For further analysis, we cast (3.1.1-2) into a dimensionless form by choosing the following scales:

- a horizontal scale  $L$  (e.g. defined by the half width of an obstacle),
- a vertical scale  $H_o$  (usually defined by the mean water depth), and
- a velocity scale (defined by the phase speed  $\sqrt{g^* H_o}$ ).

The resulting dimensionless system reads

$$\frac{Du}{Dt} + \frac{\partial(h + H)}{\partial x} = 0 \quad \text{with} \quad \frac{D}{Dt} = \frac{\partial}{\partial t} + u \frac{\partial}{\partial x} , \quad (3.1.5)$$

$$\frac{\partial H}{\partial t} + \frac{\partial(uH)}{\partial x} = 0 , \quad (3.1.6)$$

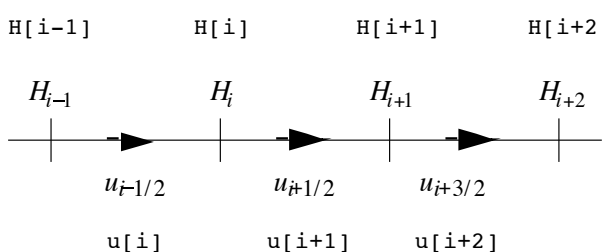
and the Froude number simplifies to  $Fr = |u|/\sqrt{H}$ .

A simple scheme to integrate the shallow-water equations uses centered differences in space and time. The accuracy of the scheme can be improved by using a *staggered grid* defined by

$$H_j^n = H(x = j\Delta x, t = n\Delta t) , \quad (3.1.10)$$

$$u_{j+1/2}^n = u(x = (j + 1/2)\Delta x, t = n\Delta t) . \quad (3.1.11)$$

Thus, the grid has the following structure:



In this staggered grid, the location of the  $u$ -grid is shifted by half a grid increment in the  $x$ -direction. The two grids points are commonly referred to as mass and velocity grids, respectively. When implementing the code on a staggered grid, care is required regarding the staggered indices. In analytical terminology, we use the notation with half integers ( $u_{i+1/2}$ ), while in the code itself only integer array indices are allowed ( $u[i+1] = u_{i+1/2}$ ).

The discretization of (3.1.5-6) on this grid, using centered differencing, yields

$$\begin{aligned} \frac{1}{2\Delta t} [u_{j+1/2}^{n+1} - u_{j+1/2}^{n-1}] + \frac{u_{j+1/2}^n}{2\Delta x} [u_{j+3/2}^n - u_{j-1/2}^n] \\ + \frac{1}{\Delta x} [(H_{j+1}^n + h_{j+1}) - (H_j^n + h_j)] = 0 \end{aligned}, \quad (3.1.12)$$

$$\begin{aligned} \frac{1}{2\Delta t} [H_j^{n+1} - H_j^{n-1}] + \frac{1}{2\Delta x} [u_{j+1}^n H_{j+1}^n - u_{j-1}^n H_{j-1}^n] = 0 \\ \text{with } u_j^n = \frac{1}{2} (u_{j-1/2}^n + u_{j+1/2}^n) \end{aligned}, \quad (3.1.13)$$

This is an explicit scheme, i.e. (3.1.12-13) can be solved for  $u^{n+1}$  and  $H^{n+1}$ .

The scheme (3.1.12-13) is stable, but in complex circumstances (e.g. hydraulic jumps), additional steps to preserve stability are needed. This may include an Asselin filter to suppress the computational mode of centered time stepping schemes, or some digital diffusion to suppress nonlinear instability (see Schär, 2006, chapters 4.3 and 5).

### 3.1.4 Integration in flux form using the Euler time step

The numerical integration (3.1.12-13) is well suited for a range of purposes (e.g. wave propagation) but it has some serious deficiencies that become important in nonlinear flows. In particular, the scheme conserves mass, but the momentum equation is not in conservative flux form, and this implies that momentum can unphysically be created or destroyed.

To suppress such artifacts, we convert (3.1.5) into its conservative flux form. To this end, we start with the product rule from differential calculus, i.e.  $\partial(Hu)/\partial t = H(\partial u/\partial t) + u(\partial H/\partial t)$ , and substitute from (3.1.5-6) to obtain

$$\frac{\partial(Hu)}{\partial t} + \frac{\partial[u(Hu)]}{\partial x} + H \frac{\partial(h+H)}{\partial x} = 0. \quad (3.1.20)$$

In absence of topography ( $h = 0$ ), the third term may be written as  $\partial(H^2/2)/\partial x$ , and this shows that (3.1.20) is in momentum conservative flux form. In particular, integration of (3.1.20) over an interval  $[a,b]$  yields

$$\frac{\partial}{\partial t} \int_a^b Hu dx = - \left[ Hu^2 + H^2/2 \right]_a^b, \quad (3.1.21)$$

This shows that the total momentum in this interval can only change in response to momentum fluxes at the boundaries. In the case of topography ( $h \neq 0$ ) however, there is some momentum exchange with the underlying surface by pressure forces. This momentum exchange is the shallow-water analog of the mountain drag (or orographic drag), which is an important term in the atmospheric momentum balance. However, even in this case, the conservative flux form (3.1.20) is preferable, as it describes the physics of the system more realistically than its advective counterpart (3.1.5).

#### INTEGRATION OF THE CONTINUITY EQUATION

The continuity equation (3.1.6) is integrated using the first-order flux form of the upstream scheme (see Schär 2006, chapter 6.3).

$$\frac{H_i^{n+1} - H_i^n}{\Delta t} + \frac{F_{i+1/2}^{n+1/2} - F_{i-1/2}^{n+1/2}}{\Delta x} = 0 \quad (3.1.23)$$

with the upstream fluxes estimated as

$$F_{i+1/2}^{n+1/2} = \begin{cases} u_{i+1/2}^n H_i^n & \text{for } u_{i+1/2}^n \geq 0 \\ u_{i+1/2}^n H_{i+1}^n & \text{for } u_{i+1/2}^n \leq 0 \end{cases}. \quad (3.1.24)$$

On the computer, this is implemented as

$$F_{i+1/2}^{n+1/2} = \text{Max}(0, u_{i+1/2}^n) H_i^n + \text{Min}(0, u_{i+1/2}^n) H_{i+1}^n \quad (3.1.25)$$

in order to avoid a case distinction (if statement). The main advantage of the staggered grid (3.1.10-11) becomes evident: it allows one to employ horizontal finite differences over  $\Delta x$  (rather than  $2\Delta x$ ) in equation (3.1.23).

#### INTEGRATION OF THE MOMENTUM EQUATION

Upon defining the momentum variable  $q := Hu$ , (3.1.20) can be written as

$$\frac{\partial q}{\partial t} + \frac{\partial(uq)}{\partial x} + H \frac{\partial(h+H)}{\partial x} = 0. \quad (3.1.26)$$

As a first step, we need to diagnose the momentum  $q$  at the mass points from the other variables as

$$q_i^n = H_i^n \frac{u_{i-1/2}^n + u_{i+1/2}^n}{2} \quad (3.1.27)$$

The simplest discretization of (3.1.26) using the flux-form of the upstream scheme then reads

$$\frac{q_i^{n+1} - q_i^n}{\Delta t} + \frac{Q_{i+1/2}^{n+1/2} - Q_{i-1/2}^{n+1/2}}{\Delta x} = H_i^n \frac{(h_{i+1} - h_{i-1}) + (H_{i+1}^n - H_{i-1}^n)}{2\Delta x} \quad (3.1.28)$$

where, analogous to (3.1.25), the upstream fluxes

$$Q_{i+1/2}^{n+1/2} = \text{Max}(0, u_{i+1/2}^n) q_i^n + \text{Min}(0, u_{i+1/2}^n) q_{i+1}^n \quad (3.1.29)$$

are employed. Once  $q_i^{n+1}$  has been computed with (3.1.28), one diagnoses the “advective velocities” on the staggered grid as

$$u_{i+1/2}^{n+1} = \frac{q_i^{n+1} + q_{i+1}^{n+1}}{H_i^{n+1} + H_{i+1}^{n+1}}. \quad (3.1.30)$$

This procedure is referred to as “momentum averaging”. It has some advantages over “velocity averaging”, which would average the diagnosed velocities at gridpoints  $i$  and  $i+1$ .

The procedure outlined above has some attractive properties. In particular, we have employed the conservative flux form, which is well suited to treat hydraulic jumps. However, the procedure also has some disadvantages. First, the use of the upstream fluxes yields a shallow-water scheme merely of first-order accuracy. Second, the treatment of the pressure gradient term is not optimal. As it employs differences over  $2\Delta x$ , spurious small-scale oscillations may result, in particular near hydraulic jumps. Both these disadvantages can be addressed using more sophisticated approaches.

### 3.2 Quasi-geostrophic dynamics

As a second example we consider the quasi-geostrophic set of equations in the Boussinesq approximation and in "pseudo-height" coordinates. This set of equations represents a simplified idealized dynamical system. Due to its conceptual elegance, it is commonly used for research purposes in large-scale geophysical dynamics. For an introduction into the quasi-geostrophic dynamics, see Holton (2004).

The system is described by few quantities, which are all closely related to the geopotential  $\phi$ : the geostrophic wind

$$(u_g, v_g) = f^{-1}(-\phi_y, \phi_x), \quad (3.2.1)$$

the quasi-geostrophic potential vorticity

$$q = \phi_{xx} + \phi_{yy} + \left( \frac{f^2}{N^2} \phi_z \right)_z \quad (3.2.2)$$

and the potential temperature

$$\Theta_o + \Theta(z) + \theta(x, y, z, t). \quad (3.2.3)$$

The latter is split into 3 terms: The first term represents a constant value that is usually associated with the Earth's surface temperature. The second term defines the mean vertical temperature profile and the Brunt-Väisällä frequency

$$N(z) = \left( \frac{g}{\Theta_o} \frac{\partial \Theta}{\partial z} \right)^{1/2}. \quad (3.2.4)$$

The third term finally defines the spatial and temporal variations around the background profile. It is linked to the geopotential by the hydrostatic relation

$$\theta = \frac{\Theta_o}{g} \frac{\partial \phi}{\partial z}. \quad (3.2.5)$$

The quasi-geostrophic dynamics in a domain  $0 \leq z \leq z_t$  is governed by the conservation of quasi-geostrophic potential vorticity inside the domain, i.e.

$$\frac{D_g q}{Dt} = 0 \quad \text{for } 0 < z < z_t, \quad (3.2.6)$$

and the conservation of potential temperature on the bounding surfaces, i.e.

$$\frac{D_g \theta}{Dt} = 0 \quad \text{for } z=0, z_t. \quad (3.2.7)$$

In the latter two equations, the advection operator accounts for the geostrophic wind

$$\frac{D_g}{Dt} = \frac{\partial}{\partial t} + u_g \frac{\partial}{\partial x} + v_g \frac{\partial}{\partial y}. \quad (3.2.8)$$

while neglecting vertical advection.

A simple numerical scheme to integrate the quasi-geostrophic system involves the following steps:

- (i) Prognosis of  $q$  inside the domain using (3.2.6).
- (ii) Prognosis of  $\theta$  on the bounding surfaces  $z = 0, z_t$  using (3.2.7).
- (iii) Quasi-geostrophic inversion: This involves solving the boundary value problem formed by (3.2.2) and (3.2.5), i.e.

$$\begin{aligned} \phi_{xx} + \phi_{yy} + \left( \frac{f^2}{N^2} \phi_z \right)_z &= q \quad \text{for } 0 \leq z \leq z_t \\ \phi_z &= \frac{g\theta}{\Theta_o} \quad \text{for } z=0, z_t \end{aligned} \tag{3.2.9}$$

with the quantities on the right-hand sides provided by the prognostic steps (i) and (ii). Equation (3.2.9) is an elliptic problem, and its solution involves iterative procedures.

- (iv) Computation of the geostrophic wind from the geopotential  $\phi$  using (3.2.1).

In distinction to the shallow-water equations, solving the quasi-geostrophic systems involves both prognostic (i,ii) and diagnostic steps (iii, iv). The latter do not include any time stepping but rather aim at the consistent diagnosis of  $\phi, u_g$  and  $v_g$ . This distinction between prognostic and diagnostic steps is typical for most atmospheric models.

### 3.3 Coordinate transformation

#### 3.3.1 Motivation

The proper choice of vertical and horizontal coordinates in atmospheric and oceanic models is an important topic. There are a large number of choices, and the optimal approach depends upon a number of factors (dynamical approximation, computational domain, model resolution, etc). Of particular importance is the choice of the vertical coordinate system, due to the presence of underlying topography. Some vertical coordinate systems are sketched in Fig.3.3.1. In absence of topography (or bathymetry in the case of the ocean), the *height coordinate* ( $z$ -coordinate system) is commonly used in non-hydrostatic models, while the *pressure coordinate* ( $p$ -coordinate) is optimal for idealized hydrostatic models.

There are two major principles that guide the choice of the vertical coordinate:

- (1) A clever choice of the vertical coordinate allows the governing equations to be greatly simplified. The choice depends upon the dynamical approximation. For the hydrostatic dynamics, the pressure coordinate (see Fig.3.3.1b) is optimal, as it leads to a considerable simplification of the governing equations. As an example consider the continuity equation. In  $z$ -coordinates (Fig.3.3.1a), it reads

$$\frac{\partial \rho}{\partial t} + \frac{\partial(\rho u)}{\partial x} + \frac{\partial(\rho v)}{\partial y} + \frac{\partial(\rho w)}{\partial z} = 0 \quad (3.3.1)$$

and exhibits a highly nonlinear structure. In pressure coordinates, the continuity equation reads

$$\left( \frac{\partial u}{\partial x} \right)_p + \left( \frac{\partial v}{\partial y} \right)_p + \frac{\partial \omega}{\partial p} = 0 \quad (3.3.2)$$

In comparison to (3.3.1), the pressure-coordinate version is diagnostic (the time-dependent term  $\partial \rho / \partial t$  disappears) and linear, and together this represents a dramatic simplification. Note that here the vertical motion is described by the vertical velocity  $\omega = Dp/Dt$  (measured in hPa/s), and horizontal derivatives are taken on surfaces of constant pressure (see later).

- (2) The coordinate system should allow for the definition of a simple numerical grid. The aforementioned pressure coordinate has an inconvenient disadvantage. The atmospheric variables are defined in the domain

$$p_s(t, x, y) > p > 0,$$

where  $p_s$  refers to surface pressure. In  $(x, y, p)$  space, the computational domain has an irregular and time-dependent lower boundary condition, as pressure surfaces intersect the ground, in particular in the presence of topography (Fig.3.3.1b). A classical

approach to this problem is the terrain-following *sigma-coordinate* (Fig.3.3.1c) It is defined as

$$\sigma := \frac{p}{p_s} . \quad (3.3.3)$$

With this choice, grid points are located on surfaces defined by  $\sigma = \text{const}$ . The coordinate  $\sigma$  runs from  $\sigma=0$  (at the top of the atmosphere defined by  $p=0$ ) to  $\sigma=1$  (at the Earth's surface defined by  $p=p_s$ ). This yields a regular computational domain

$$1 > \sigma > 0 .$$

The deformation of  $\sigma$ -coordinates that results from underlying topography decays with height. Sigma-coordinates are also suited for oceanic models. However, to avoid collapsing computational surfaces near coast lines, vertical walls must be introduced (Fig.3.3.1d). This implies neglecting the continental shelf.

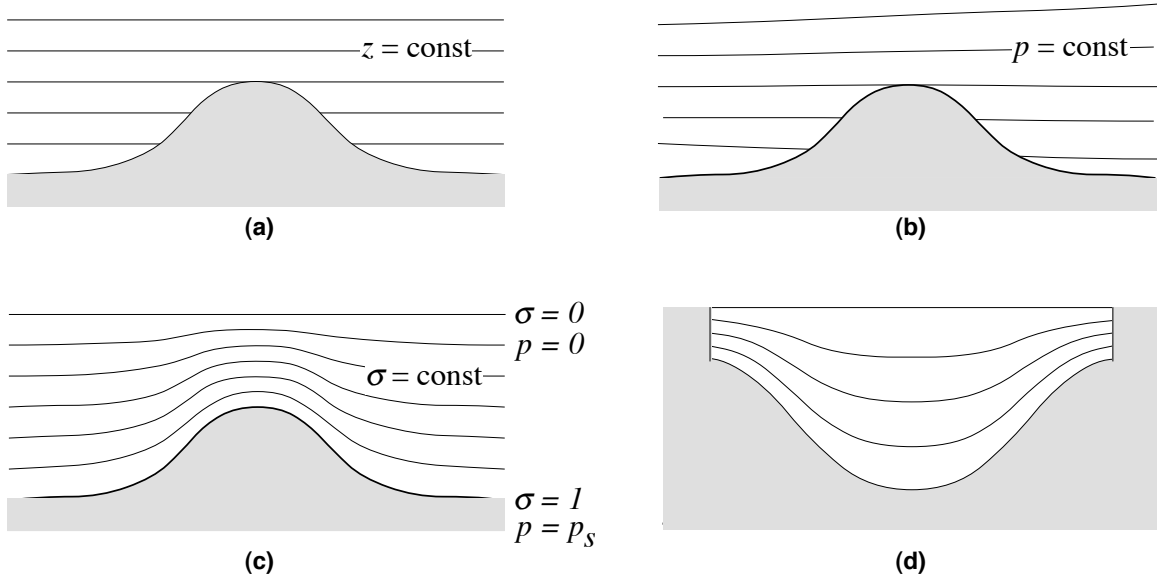


**Fig.3.3.1:** Examples of vertical coordinate systems: (a)  $z$ -coordinates, (b)  $p$ -coordinates, (c)  $\sigma$ -coordinates in atmospheric models, (d)  $\sigma$ -coordinates in oceanic models.

In addition to the coordinate systems considered above, there is a large variety of additional coordinates:

- Isentropic coordinate systems adopt potential temperature  $\theta$  as vertical coordinate (see section 3.5). This system is particularly attractive for idealized dynamical studies, and closely related to isosteric coordinates (where density  $\rho$  serves as vertical coordinate).
- Hybrid coordinates typically use terrain-following  $\sigma$ -coordinates at low levels, with a smooth transition to  $p$ -coordinates and/or  $\theta$ -coordinates at upper levels.
- In the context of finite-volume atmospheric models, there is some recent research about variants of  $z$ -coordinates (e.g. the shaved-cell approach).

Coordinate transformations are also important in order to represent the spherical geometry of the planet. On a sphere, a simple Cartesian coordinate system does not exist. Common meteorological convention defines a local Cartesian  $(x,y,z)$ , where the  $z$ -axis points upwards, and the  $x$ -axis towards east. This coordinate system is closely related to the spherical  $(\lambda,\phi,z)$ -system. In these lecture notes we will – except for section 3.7 – restrict attention to the f-plane approximation and thus mostly work with a Cartesian  $(x,y,\tilde{z})$ -system where  $\tilde{z}$  denotes a generalized vertical coordinate. However, the proper representation of the spherical geometry is an important topic, in atmospheric and oceanic models.

The implementation of an atmospheric or oceanic model in generalized coordinates  $(\tilde{x},\tilde{y},\tilde{z})$  involves two steps. In a first step, the governing equations need to be transformed into the new coordinate system. In a second step, a discretization is introduced, for instance by using grid increments  $(\Delta\tilde{x},\Delta\tilde{y},\Delta\tilde{z})$  in the new coordinate directions.

### 3.3.2 Wind vector and advection operator in generalized coordinates

We consider the transformation of a Cartesian coordinate system  $(x,y,z)$  into a (generally non-Cartesian) coordinate system  $(\tilde{x},\tilde{y},\tilde{z})$ . To this end, we first need a precise definition of the wind vector. In Cartesian coordinates  $(x,y,z)$  the definition reads

$$u := \frac{Dx}{Dt}, \quad v := \frac{Dy}{Dt}, \quad w := \frac{Dz}{Dt}, \quad (3.3.10a)$$

and it can readily be generalized to an arbitrary (curvilinear) coordinate system  $(\tilde{x},\tilde{y},\tilde{z})$ :

$$\tilde{u} := \frac{D\tilde{x}}{Dt}, \quad \tilde{v} := \frac{D\tilde{y}}{Dt}, \quad \tilde{w} := \frac{D\tilde{z}}{Dt}. \quad (3.3.10b).$$

The wind vector is thus defined by the rate of change with time of the air parcel's location. The advection operator  $D/Dt$  appearing in (3.3.10) is the usual total derivative used in fluid dynamics.

According to (3.3.10b), the vertical wind in  $(\tilde{x},\tilde{y},\tilde{z})=(x,y,p)$  coordinates is defined as

$$\omega := \frac{Dp}{Dt}, \quad (3.3.11)$$

and measured in [hPa/s]. Note that it is negative (positive) for ascending (descending) motions. Similarly, the vertical wind in isentropic coordinates  $(\tilde{x},\tilde{y},\tilde{z})=(x,y,\theta)$  is defined as

$$\dot{\theta} := \frac{D\theta}{Dt}. \quad (3.3.12)$$

and measured in [K/s]. Note that for this system  $\dot{\theta} \neq 0$  implies the presence of diabatic processes, as for the adiabatic dynamics the potential temperature is conserved following the motion of the flow, i.e.  $D\theta/Dt = 0$ . For adiabatic flows, the vertical velocity component thus vanishes, i.e.  $\mathbf{v}=(u,v,0)$ .

The advection operator can be formed in generalized coordinates using the total derivative. In the  $(x,y,z)$ -system this reads

$$\begin{aligned}\frac{D}{Dt} &= \frac{\partial}{\partial t} + \frac{Dx}{Dt} \left( \frac{\partial}{\partial x} \right)_{y,z} + \frac{Dy}{Dt} \left( \frac{\partial}{\partial y} \right)_{x,z} + \frac{Dz}{Dt} \left( \frac{\partial}{\partial z} \right)_{x,y} \\ &= \frac{\partial}{\partial t} + u \left( \frac{\partial}{\partial x} \right)_{y,z} + v \left( \frac{\partial}{\partial y} \right)_{x,z} + w \left( \frac{\partial}{\partial z} \right)_{x,y}\end{aligned}\quad (3.3.13a)$$

and in the generalized  $(\tilde{x},\tilde{y},\tilde{z})$ -system

$$\begin{aligned}\frac{D}{Dt} &= \frac{\partial}{\partial t} + \frac{D\tilde{x}}{Dt} \left( \frac{\partial}{\partial \tilde{x}} \right)_{\tilde{y},\tilde{z}} + \frac{D\tilde{y}}{Dt} \left( \frac{\partial}{\partial \tilde{y}} \right)_{\tilde{x},\tilde{z}} + \frac{D\tilde{z}}{Dt} \left( \frac{\partial}{\partial \tilde{z}} \right)_{\tilde{x},\tilde{y}} \\ &= \frac{\partial}{\partial t} + \tilde{u} \left( \frac{\partial}{\partial \tilde{x}} \right)_{\tilde{y},\tilde{z}} + \tilde{v} \left( \frac{\partial}{\partial \tilde{y}} \right)_{\tilde{x},\tilde{z}} + \tilde{w} \left( \frac{\partial}{\partial \tilde{z}} \right)_{\tilde{x},\tilde{y}}\end{aligned}\quad (3.3.13b)$$

Here we have used the usual convention of partial differential calculus and employ subscripts to define the coordinates that are held constant when forming derivatives. For ease of notation, subscripts are suppressed unless they are needed to avoid confusion. For instance, when considering the two systems  $(x,y,z)$  and  $(\tilde{x},\tilde{y},\tilde{z}) = (x,y,p)$ , we simplify the notation as follows:  $(\partial/\partial x)_p = (\partial/\partial x)_{y,p}$  and  $\partial/\partial p = (\partial/\partial p)_{x,y}$ .

### 3.3.3 Transformation of derivatives with generalized coordinates

Most coordinate systems of relevance to atmospheric and oceanic models belong to the class of *curvilinear coordinates*. Simple examples of curvilinear coordinates include polar or spherical coordinates. The definition of “curvilinear” requires that these coordinates are locally invertible and differentiable, but the coordinate surfaces may be curved and non-Cartesian.

When transforming the governing system of equations from Cartesian to general curvilinear coordinates, we need to eliminate the coordinates  $(x,y,z)$  and to express the derivatives in terms of the new coordinates. For instance, when considering the generalized three-dimensional coordinate transformation, we need to express the derivative  $(\partial/\partial x)_{y,z}$  in terms of  $(\partial/\partial \tilde{x})_{\tilde{y},\tilde{z}}$ ,  $(\partial/\partial \tilde{y})_{\tilde{x},\tilde{z}}$  and  $(\partial/\partial \tilde{z})_{\tilde{x},\tilde{y}}$ . In the general case, this task requires tensor calculus (e.g. Fletcher 1991).

However, here we restrict attention to transformations of the vertical coordinate assuming horizontal Cartesian coordinates  $(x,y)$  in *f*-plane geometry. In this case, the coordinate transformations are much simpler and tensor calculus is not needed. In this simplified framework, a new vertical coordinates may be defined by a function

$$s = s(x,y,z)$$

At each location  $(x,y)$ , the function  $s(z)$  must be strictly monotonic in  $z$  to guarantee an invertible coordinate system. To address the associated transformation  $(x,y,z) \Leftrightarrow (x,y,s)$ , we consider derivatives of some quantity  $\chi = \chi(x,y,z) = \chi(x,y,s)$ .

For *vertical derivatives*, the transformation from the  $z$ - to the  $s$ -system can be accomplished using the chain rule i.e.

$$\frac{\partial \chi}{\partial s} = \frac{\partial \chi}{\partial z} \frac{\partial z}{\partial s}, \quad (3.3.20)$$

where the factor  $\partial z / \partial s$  can be determined from  $s = s(x,y,z)$ .

For *horizontal derivatives*, we need to represent the fact that horizontal derivatives are taken on  $z$ - and  $s$ -surfaces, respectively. To this end, consider variations of  $\chi(x,y,s)$  in an environment around  $(x_0, y_0, s_0)$ . Wandering around in this environment with  $(\delta x \neq 0, \delta y = 0, \delta s)$ , implies variations of  $\chi$  given by

$$\delta \chi = \left( \frac{\partial \chi}{\partial x} \right)_s \delta x + \left( \frac{\partial \chi}{\partial s} \right) \delta s.$$

Here the subscript  $s$  denotes a derivative on an  $s$ -surface. Division by  $\delta x$  yields

$$\frac{\delta \chi}{\delta x} = \left( \frac{\partial \chi}{\partial x} \right)_s + \frac{\partial \chi}{\partial s} \left( \frac{\delta s}{\delta x} \right).$$

Next we assume that  $\delta x$  and  $\delta s$  depend upon each other such that  $\delta z = 0$ ; this means we restrict our attention to walks on  $z$ -surfaces. It follows that  $\delta/\delta x$  may be replaced by  $(\partial/\partial x)_z$ , i.e.

$$\left( \frac{\partial \chi}{\partial x} \right)_z = \left( \frac{\partial \chi}{\partial x} \right)_s + \frac{\partial \chi}{\partial s} \left( \frac{\partial s}{\partial x} \right)_z \quad (3.3.21)$$

This equation allows converting a horizontal derivative on a  $z$ -surface by a horizontal derivative on an  $s$ -surface.

Equations (3.3.20) and (3.3.21) are completely general. We have not made any assumptions, not even that  $(x,y,z)$  is a Cartesian system. It follows that  $s$  and  $z$  can be arbitrarily exchanged with each other, or replaced by other symbols (e.g. by  $p$  or  $\theta$ ). The only important assumption is that the transformation  $s = s(x,y,z)$  is invertible and continuous.

### 3.3.4 Transformation of the horizontal momentum equation

As example we next consider the transformation of the hydrostatic momentum equations in pressure coordinates on an  $f$ -plane. The respective equations in  $z$ -coordinates read

$$\frac{Du}{Dt} - fv = -\frac{1}{\rho} \frac{\partial p}{\partial x} \quad (3.3.22a)$$

$$\frac{Dv}{Dt} + fu = -\frac{1}{\rho} \frac{\partial p}{\partial y} \quad (3.3.22b)$$

Here  $p$  denotes pressure,  $\rho$  is density, and  $f = 2\Omega \sin(\phi)$  denotes the Coriolis-parameter with  $\Omega = 2\pi/24h$  the angular velocity of the Earth's rotation and  $\phi$  the geographical latitude.

The full form of the advection operator reads

$$\frac{D}{Dt} = \frac{\partial}{\partial t} + u \frac{\partial}{\partial x} + v \frac{\partial}{\partial y} + w \frac{\partial}{\partial z} \quad (3.3.23)$$

with  $\mathbf{u} = (u, v, w)$  representing the three-dimensional velocity vector.

As the transformation to pressure coordinates does not affect  $(x, y)$ , the horizontal velocity components  $(u, v)$  are unchanged. However, in place of the Cartesian vertical wind  $w$  [m/s], we use the vertical wind "omega"  $\omega = Dp/Dt$  [hPa/s] as discussed in section 3.3.2. Thus, the left-hand side of equation (3.3.22) remains unchanged, except for a modified form of the advection operator

$$\frac{D}{Dt} = \frac{\partial}{\partial t} + u \left( \frac{\partial}{\partial x} \right)_p + v \left( \frac{\partial}{\partial y} \right)_p + \omega \frac{\partial}{\partial p} \quad (3.3.24)$$

In order to transform the pressure gradient terms on the right-hand side of (3.3.22), we next use (3.3.21), where we replace  $z$  by  $p$  and  $s$  by  $z$ , i.e.

$$\left( \frac{\partial \chi}{\partial x} \right)_p = \left( \frac{\partial \chi}{\partial x} \right)_z + \frac{\partial \chi}{\partial z} \left( \frac{\partial z}{\partial x} \right)_p .$$

Replacing  $\chi$  by  $p$  implies

$$\left( \frac{\partial p}{\partial x} \right)_p = \left( \frac{\partial p}{\partial x} \right)_z + \frac{\partial p}{\partial z} \left( \frac{\partial z}{\partial x} \right)_p \Rightarrow \left( \frac{\partial p}{\partial x} \right)_z = -\frac{\partial p}{\partial z} \left( \frac{\partial z}{\partial x} \right)_p = g\rho \left( \frac{\partial z}{\partial x} \right)_p$$

where we have used  $(\partial p / \partial x)_p = 0$  and the hydrostatic relation  $\partial p / \partial z = -g\rho$ . The transformed version of (3.3.22a) then follows

$$\frac{Du}{Dt} - fv = -g \left( \frac{\partial z}{\partial x} \right)_p$$

Here  $z=z(x, y, p, t)$  refers to the height of a pressure surface, and it replaces  $p=p(x, y, z, t)$  in the  $z$ -coordinate version. The preceding equation is usually rewritten using the definition of the geopotential  $\phi=gz$ , i.e.

$$\frac{Du}{Dt} - fv = - \left( \frac{\partial \phi}{\partial x} \right)_p \quad (3.3.25)$$

The latter form is somewhat more general, as it allows for variations of gravity, i.e.  $g=g(x, y, z)$ .

Comparison of (3.3.22a) and (3.3.25) shows a dramatic simplification of the pressure gradient term, as the density factor  $1/\rho$  has disappeared. This is another important advantage of pressure coordinates over height coordinates, beyond those discussed in section 3.3.1

### 3.4 Hydrostatic dynamics in pressure coordinates

We consider the atmospheric equations of motion in their hydrostatic approximation. Most numerical weather prediction models and virtually all climate models are based on this set of equations, although non-hydrostatic atmospheric models are rapidly gaining importance in high-resolution (kilometer-scale) modeling. We consider the equations in their adiabatic / inviscid and dry form. For the moment we also neglect effects associated with the spherical geometry of the Earth and consider a form of the equations that is commonly used in regional (limited-area) weather and climate models. We begin by considering the equations in pressure coordinates, and later consider the numerical integration in  $\theta$ -coordinates (chapter 3.5) und  $\sigma$ -coordinates (chapter 3.6).

The dynamics and thermodynamics of a dry atmosphere are defined by the following three-dimensional time-dependent fields of the form  $\chi = \chi(x, y, p, t)$ :

- $u, v$  horizontal velocity components,
- $\omega$  vertical velocity ( $\omega = Dp / Dt$ ),
- $\phi = gz$  geopotential,
- $\rho$  density, and
- $T$  temperature.

and by one two-dimensional field:

$$p_s(x, y, t) \quad \text{surface pressure.}$$

The governing system of equations is presented here without derivation (except for the horizontal momentum equations considered in section 3.3). Succinct derivations can be found in Holton (2004) or Gill (1982).

The governing equations include the equation of state

$$p = \rho RT , \tag{3.4.1}$$

the continuity equation

$$\left( \frac{\partial u}{\partial x} \right)_p + \left( \frac{\partial v}{\partial y} \right)_p + \frac{\partial \omega}{\partial p} = 0 , \tag{3.4.2}$$

the thermodynamic equation

$$\frac{DT}{Dt} = \frac{\omega}{\rho c_p} + \frac{Q}{c_p} , \tag{3.4.3}$$

the hydrostatic equation

$$\frac{\partial \phi}{\partial p} = -\frac{1}{\rho} , \tag{3.4.4}$$

and the horizontal momentum equations (3.3.25)

$$\frac{Du}{Dt} - fv = - \left( \frac{\partial \phi}{\partial x} \right)_p + F^x , \quad (3.4.5a)$$

$$\frac{Dv}{Dt} + fu = - \left( \frac{\partial \phi}{\partial y} \right)_p + F^y , \quad (3.4.5b)$$

All "horizontal" derivatives in (3.4.1-5) are to be taken on surfaces of constant pressure, and the advection operator is defined by

$$\frac{D}{Dt} = \frac{\partial}{\partial t} + u \left( \frac{\partial}{\partial x} \right)_p + v \left( \frac{\partial}{\partial y} \right)_p + \omega \frac{\partial}{\partial p} , \quad (3.4.6)$$

The non-conservative force  $\mathbf{F} = (F^x, F^y)$  and the diabatic heating rate  $Q$  relate to processes that are not explicitly represented above (moist dynamics, atmospheric radiation, turbulence, boundary layer processes, etc). For the moment we assume that these terms are externally specified or vanish. Later we will learn how  $\mathbf{F}$  and  $Q$  are represented by parameterizations. Note also that in the above form the governing equations allow variations of the Earth's acceleration  $g$  (which are particularly important if a deep atmosphere is considered), but for simplicity we will subsequently assume that  $g=const.$

Solving the governing equations (3.4.1-5) requires three boundary conditions. The first is the geometric lower boundary condition

$$\phi(p = p_s) = g z_s \quad (3.4.7)$$

that matches for the height  $z_s = z_s(x, y)$  of the underlying topography with the geopotential. The second is the kinematic boundary condition at the top of the atmosphere, i.e.

$$\omega(p = 0) = 0 . \quad (3.4.8)$$

It ensures that vertical motions vanish at the top of the atmosphere ( $p=0$ ). The third is the kinematic boundary condition at the surface, i.e.

$$\omega(p = p_s) = \partial p_s / \partial t + \mathbf{v}_s \cdot \nabla_h p_s \quad (3.4.9)$$

where  $\mathbf{v}_s = (u_s, v_s)$  denotes the horizontal velocity at the surface. Equation (3.4.9) ensures that the three-dimensional velocity vector at the surface must always be tangential to the surface. The notion of a tangential flow in the  $p$ -system is somewhat obscured by the fact that the surface pressure  $p=p_s(x, y, t)$  may vary with time. The boundary condition can be derived from (3.3.11) after noting that  $p$  may be replaced by  $p_s$  (as the respective air parcel must remain at the surface) and that  $\partial p_s / \partial p = 0$  (as the surface pressure  $p_s$  does not depend upon the vertical coordinate  $p$ ).

## 3.5 Isentropic coordinates

### 3.5.1 Background

In the isentropic system, the potential temperature  $\theta$  serves as the vertical coordinate. The potential temperature of an air parcel is defined as the temperature that the parcel would acquire if adiabatically brought to the reference pressure  $p_{ref} = 1000$  hPa. Thermodynamics of ideal gases yields

$$\theta = T \left( \frac{p_{ref}}{p} \right)^{\frac{R}{c_p}}, \quad (3.5.1)$$

where  $R = 287$  J/(K kg) denotes the gas constant for dry air, and  $c_p = 1004$  J/(K kg) the specific heat of dry air at constant pressure.

The potential temperature is a very useful concept. By definition, potential temperature is conserved following adiabatic motions, i.e.  $D\theta/Dt = 0$ . As many atmospheric flows are approximately adiabatic (i.e. cyclogenesis or flow past topography), air parcels retain their potential temperature (while experience a change in temperature), even when undergoing ascent or descent in some atmospheric motions. The vertical wind in isentropic coordinates is defined

$$\dot{\theta} := \frac{D\theta}{Dt} \quad (3.5.2)$$

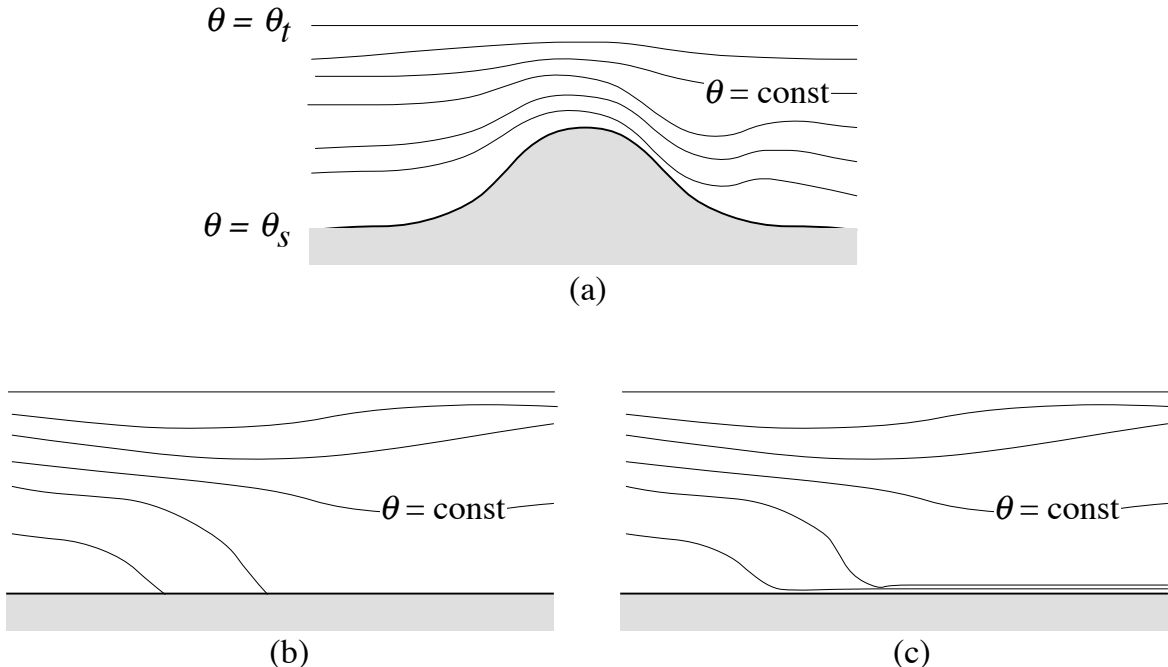


**Fig.3.5.1:** Vertical sections of isentropic coordinates in (a) an idealized stratified flow over a mountain, and (b,c) in a frontal zone. Panel (c) shows how the lower boundary condition may be represented by theta-layers of vanishing thickness (see text).

and is measured in [K/s]. For adiabatic flows  $\dot{\theta} = D\theta/Dt=0$ , i.e. the vertical wind vanishes and the flow becomes quasi-horizontal on the  $\theta$ -surfaces. This is an important simplification in numerical implementations. Isentropic coordinates are thus well suited for idealized studies of adiabatic flows. However, the invertibility condition of coordinate transformations requires that  $\theta = \theta(z)$  and  $\theta = \theta(p)$  are strictly monotonic functions, i.e.

$$\frac{\partial \theta}{\partial z} > 0 \quad \text{and} \quad \frac{\partial \theta}{\partial p} < 0 . \quad (3.5.3)$$

These conditions are often not met in the lower troposphere or in the planetary boundary layer. Thus, isentropic coordinates are not suited for realistic weather prediction or climate models, or only in combination with other coordinates (e.g.  $\sigma$ - $p$ - $\theta$  hybrid coordinate, see Zhu et al. 1992).

An additional disadvantage of isentropic coordinates is due to notorious difficulties at the lower boundary. For certain idealized problems (such as adiabatic flows past mountain ridges) the lower boundary may be represented by a surface of constant potential temperature (see Fig.3.5.1a). In general, however, atmospheric flows are baroclinic (e.g. horizontal temperature gradients in frontal zones) and the lower boundary contains some temperature contrast (Fig.3.5.1b). In these cases, near-surface isentropic layers may be represented as collapsed massless layers (see Fig.3.5.1c), which yields a difficult numerical problem.

### 3.5.2 Isentropic form of governing equations

#### (A) ADVECTIVE FORM OF MOMENTUM EQUATION

The horizontal momentum equations in pressure coordinates may be expressed as

$$\frac{D\mathbf{v}}{Dt} + f \mathbf{k} \times \mathbf{v} = -\nabla_p \phi \quad (3.5.6)$$

where  $\mathbf{v} = (u, v)$  denotes the horizontal wind vector,  $\nabla_p \phi$  the pressure gradient on  $p$ -surfaces, and  $\mathbf{k}$  the vertical unit vector. The left-hand side of this equation has the same form in isentropic coordinates, but employs the appropriate advection operator, i.e.

$$\frac{D}{Dt} = \frac{\partial}{\partial t} + u \left( \frac{\partial}{\partial x} \right)_\theta + v \left( \frac{\partial}{\partial y} \right)_\theta + \dot{\theta} \frac{\partial}{\partial \theta} \quad (3.5.7)$$

For the transformation of the pressure force  $(\partial\phi/\partial x)_p$ , we use (3.3.21) after replacing  $z$  by  $\theta$ ,  $s$  by  $p$ , and  $\chi$  by  $\phi$ . This yields

$$\left( \frac{\partial \phi}{\partial x} \right)_\theta = \left( \frac{\partial \phi}{\partial x} \right)_p + \frac{\partial \phi}{\partial p} \left( \frac{\partial p}{\partial x} \right)_\theta .$$

After introducing  $\partial\phi/\partial p=-1/\rho$  from the hydrostatic relation (3.4.4), and substituting  $1/\rho=RT/p$  from the equation of state (3.4.1), and after rearranging the terms, one obtains

$$\left( \frac{\partial \phi}{\partial x} \right)_p = \left( \frac{\partial \phi}{\partial x} \right)_\theta + \frac{RT}{p} \left( \frac{\partial p}{\partial x} \right)_\theta .$$

Finally we use the definition of potential temperature (3.5.1) to eliminate pressure from the equation. Manipulation of the respective term yields

$$\frac{RT}{p} \left( \frac{\partial p}{\partial x} \right)_\theta = \frac{RT}{p_{ref}} \left( \frac{\theta}{T} \right)^{c_p/R} p_{ref} \left( \frac{\partial}{\partial x} \right)_\theta \left( \frac{T}{\theta} \right)^{c_p/R} = \left( \frac{\partial c_p T}{\partial x} \right)_\theta .$$

and

$$\frac{Du}{Dt} - fv = - \left( \frac{\partial M}{\partial x} \right)_\theta \quad (3.5.8a)$$

$$\frac{Dv}{Dt} + fu = - \left( \frac{\partial M}{\partial y} \right)_\theta \quad (3.5.8b)$$

where

$$M = \phi + c_p T = gz + c_p T \quad (3.5.9)$$

denotes the Montgomery potential. The Montgomery potential in isentropic coordinates plays the same role as the geopotential in pressure coordinates.

#### (B) ISENTROPIC MASS DENSITY AND CONTINUITY RELATION

The mass between two isentropic surfaces, i.e.  $\rho dz$ , can be derived from the hydrostatic relation as

$$\rho dz = - \frac{1}{g} \frac{\partial p}{\partial z} dz = - \frac{1}{g} \frac{\partial p}{\partial z} \frac{\partial z}{\partial \theta} d\theta = - \frac{1}{g} \frac{\partial p}{\partial \theta} d\theta .$$

It is common to define the *isentropic mass density* (or *isentropic density*)

$$\sigma = - \frac{1}{g} \frac{\partial p}{\partial \theta} , \quad (3.5.11)$$

whereupon

$$dp = \rho dz = \sigma d\theta . \quad (3.5.12)$$

Note that the isentropic density should not be mistaken for the  $\sigma$ -coordinate mentioned in section 3.1 and treated in section 3.6.

The isentropic density  $\sigma$  plays the same role as density  $\rho$  in  $z$ -coordinates. Thus, one can guess the isentropic continuity equation from the  $z$ -coordinate version (3.3.2) as

$$\frac{\partial \sigma}{\partial t} + \left( \frac{\partial \sigma u}{\partial x} \right)_\theta + \left( \frac{\partial \sigma v}{\partial y} \right)_\theta + \frac{\partial \sigma \dot{\theta}}{\partial \theta} = 0 . \quad (3.5.13)$$

The formal derivation of this equation is, however, quite cumbersome.

#### (C) HYDROSTATIC RELATION

To derive the isentropic form of the hydrostatic equation, we begin with a logarithmic version of (3.5.1), i.e.

$$\ln \theta = \ln T - \frac{R}{c_p} \ln p + \frac{R}{c_p} \ln p_{ref} .$$

Taking the derivative with respect to  $\theta$  and rearranging the terms yields

$$\frac{c_p T}{\theta} = c_p \frac{\partial T}{\partial \theta} - \frac{RT}{p} \frac{\partial p}{\partial \theta} .$$

Finally we use the hydrostatic equation in  $z$ -coordinates  $\partial p / \partial z = -g\rho$  and the gas equation to obtain

$$\frac{c_p T}{\theta} = \frac{\partial}{\partial \theta} (c_p T + gz) .$$

Comparison with (3.5.9) shows that this can be expressed as

$$\frac{c_p T}{\theta} = \frac{\partial M}{\partial \theta} \quad \text{or} \quad c_p \left( \frac{p}{p_{ref}} \right)^{R/c_p} = \frac{\partial M}{\partial \theta} \quad (3.5.14)$$

where the second form is obtained after substitution from (3.5.1).

#### (D) FLUX FORM OF MOMENTUM EQUATIONS

As with the shallow water system (chapter 3.1.3), equations (3.5.8) and (3.5.13) can be combined to derive a conservative flux from of the momentum equation. In the x-direction this is

$$\frac{\partial(\sigma u)}{\partial t} + \left( \frac{\partial(u\sigma u)}{\partial x} \right)_\theta + \left( \frac{\partial(v\sigma u)}{\partial y} \right)_\theta + \frac{\partial(\dot{\theta}\sigma u)}{\partial \theta} - f\sigma v = -\sigma \left( \frac{\partial M}{\partial x} \right)_\theta . \quad (3.5.15)$$

#### (E) BOUNDARY CONDITIONS

As with  $p$ -coordinates, integrating the governing equations requires appropriate boundary conditions at the surface and the top of the modeling domain. In the case of an adiabatic flow problem without large-scale temperature gradients (such as in Fig.3.5.1), one can assume that the domain is confined at the surface and the model top by quasi-horizontal surfaces of constant potential temperature  $\theta_s$  and  $\theta_t$ , respectively. We may assume that the top surface is horizontal (rigid lid) and characterized by constant pressure, i.e.

$$p(\theta = \theta_t) = p_t = const . \quad (3.5.16)$$

At the lower boundary, the height of the topography determines the geopotential, as in pressure coordinates, i.e.

$$\phi(\theta = \theta_s) = gz_s . \quad (3.5.17)$$

### 3.5.3 Numerical integration

The momentum equation in advective (3.5.8) or flux form (3.5.15), the continuity equation (3.5.13), the hydrostatic relation (3.5.14), the definition of the isentropic density (3.5.11), and the boundary conditions (3.5.16-17) together yield a complete prognostic set of governing equations. Here a simple numerical scheme is presented that employs ideas familiar from the treatment of the shallow water equations in chapter 3.1. However, in addition to the horizontal staggering, the variables are now also staggered in the vertical direction. The distribution of grid points in a three-dimensional isentropic model is sketched in Fig.3.5.2.

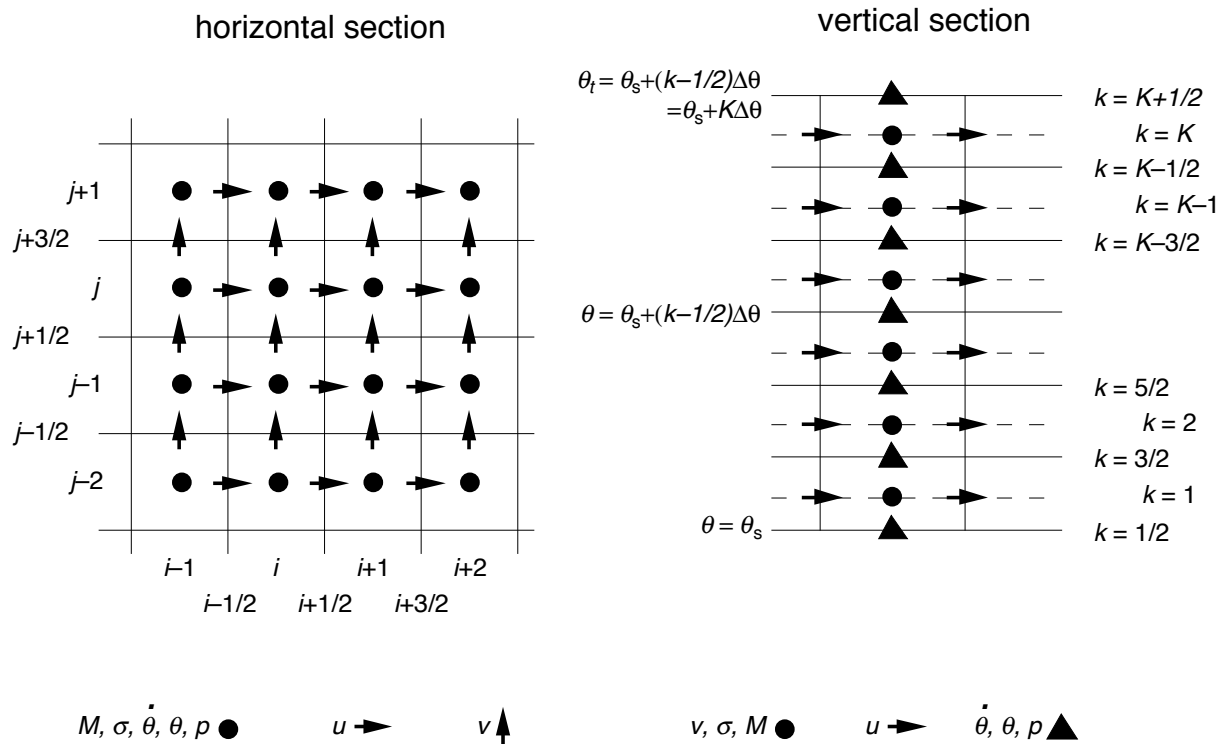


**Fig.3.5.2:** Grid points and variables in a simple three-dimensional isentropic model.

In order to simplify the situation, we will make the following additional assumptions:

- two-dimensional case in ( $\partial/\partial y=0$ ),
- adiabatic and inviscid flow ( $\dot{\theta} \equiv 0$ ),
- neglect Earth's rotation ( $f = 0$ ), and
- the lower boundary is an isentropic surface ( $\theta_s = \text{const}$ ).

The associated primary model variables are

$u_{i+1/2, k}$	horizontal wind velocity,
$\sigma_{i, k}$	isentropic mass density,
$M_{i, k}$	Montgomery potential, and
$p_{i, k+1/2}$	pressure.

Below we assume that all quantities are known at time  $t = n\Delta t$ . Below the different phases of a time step are discussed:

#### (A) PROGNOSTIC TIME STEP FOR ISENTROPIC DENSITY AND MOMENTUM

In a first step we address the approximated form of (3.5.8a) and (3.5.13), i.e.

$$\frac{\partial u}{\partial t} + u \frac{\partial u}{\partial x} = - \left( \frac{\partial M}{\partial x} \right)_{\theta}, \quad (3.5.21)$$

$$\frac{\partial \sigma}{\partial t} + \left( \frac{\partial \sigma u}{\partial x} \right)_{\theta} = 0. \quad (3.5.22)$$

These equations exhibit a remarkable similarity with the shallow-water equations (chapter 3.1), but the isentropic system is fully two-dimensional in the  $(x,z)$ -space. Upon introducing a vertical discretization of the form

$$\chi_k = \chi[\theta = \theta_s + (k - 1/2)\Delta\theta]$$

for all variables appearing in (3.5.21-22), the relationship with the shallow-water equations becomes even more apparent: The equations in each isentropic layer  $k$  are formally identical with the shallow-water equations (3.1.5-6). The role of the shallow-water layer depth  $H$  is played by the isentropic density  $\sigma$ . The only relevant difference between the two systems concerns the appearance of the Montgomery potential in the pressure term. This couples the different layers to each other, and the isentropic system can be interpreted (and treated) as a vertical stack of shallow-water equations.

The time step for each isentropic layer (3.5.21-22) can employ the same methods as used with the shallow water equations. Both the advective (chapter 3.1.2) or the flux form approach (chapter 3.1.3) may be used. This step delivers values of  $\sigma^{n+1}$  and  $u^{n+1}$  at time  $n+1$ .

#### (B) DIAGNOSIS OF PRESSURE

In distinction to the shallow-water equations, the isentropic system supports vertical coupling and wave propagation. The coupling between the different layers is instantaneously communicated vertically by the hydrostatic equation. The remaining equations (3.5.11) and (3.5.14) do not contain any time derivatives: they represent purely *diagnostic equations*. Together with the boundary condition, they allow one to compute the Montgomery potential  $M^{n+1}$  from the results of the previous step (i.e.  $\sigma^{n+1}$  and  $u^{n+1}$ ).

To begin with, the pressure is diagnosed with the help of the isentropic density (3.5.11). A vertically discretized form of this equation, using centered differencing, reads

$$\sigma_{i,k}^{n+1} = - \frac{p_{i,k+1/2}^{n+1} - p_{i,k-1/2}^{n+1}}{g \Delta\theta},$$

which can be cast into the form

$$p_{i,k-1/2}^{n+1} = p_{i,k+1/2}^{n+1} + g\Delta\theta\sigma_{i,k}^{n+1} \quad \text{for } (k=K, \dots, 1). \quad (3.5.24)$$

This equation can be evaluated from the top to the surface, starting with  $k=K$ . The uppermost pressure value that is needed for the first step is available from the upper boundary condition (3.5.16), i.e.

$$p_{i,K+1/2}^{n+1} = p_t .$$

As a result, the complete pressure distribution at time  $n+1$  becomes known.

### (C) DIAGNOSIS OF MONTGOMERY POTENTIAL

The diagnostic computation of the Montgomery potential using the hydrostatic relation (3.5.14) uses essentially the same idea. To simplify the notation, we introduce the Exner function

$$\pi(p) := c_p \left( \frac{p}{p_{ref}} \right)^{R/c_p} \quad (3.5.25)$$

whereupon the hydrostatic relation (3.5.14) simplifies to

$$\pi = \frac{\partial M}{\partial \theta} . \quad (3.5.26)$$

As we were able to compute  $p^{n+1}$  in step (B) above, we are also able to compute  $\pi^{n+1}$  using (3.5.25). Using centered finite differencing, (3.5.26) can next be discretized as

$$M_{i,k}^{n+1} = M_{i,k-1}^{n+1} + \Delta\theta\pi_{i,k-1/2}^{n+1} \quad \text{for } (k=2, \dots, K). \quad (3.5.27)$$

The plan is thus to integrate this equation from the surface to the top, starting with  $k=2$ .

Before proceeding with the first step  $k=2$  of the integration (3.5.27), we need to make use of the lower boundary condition (3.5.17) to provide  $M_{i,k=1}^{n+1}$ . The lower boundary condition provides the geopotential as  $\phi_s = gz_s$ . This is used in combination with the surface pressure from step (B) above to compute the surface Montgomery potential as

$$M_s = c_p T_s + gz_s = \theta_s \pi_s + gz_s . \quad (3.5.28)$$

In deriving (3.5.28), one starts with the definition of the Montgomery potential (3.5.9) and replaces the surface temperature by substitution from (3.5.1). Expressing (3.5.28) in numerical terms yields

$$M_{i,k=1/2}^{n+1} = \theta_s \pi_{i,k=1/2}^{n+1} + gz_s \quad (3.5.29)$$

A simple complication arises, as we need the Montgomery potential in (3.5.28) at  $M_{i,k=1}^{n+1}$  (i.e. at the center of the lowermost layer, see also Fig.3.5.2), while (3.5.29) provides it at  $M_{i,k=1/2}^{n+1}$ . In order to estimate  $M_{i,k=1}^{n+1}$ , one can use another discretized version of (3.5.26), i.e.

$$M_{i,k=1}^{n+1} = M_{i,k=1/2}^{n+1} + \frac{\Delta\theta}{2} \pi_{i,k=1/2}^{n+1} . \quad (3.5.30)$$

This equation uses a vertical stencil of  $\Delta\theta/2$  rather than  $\Delta\theta$  as in (3.5.27).

Once  $M_{i,k=1}^{n+1}$  is known from (3.5.30), we can use (3.5.27) iteratively from  $k=2$  to  $k=K$  and compute the Montgomery potential at all mass points. As a result, all primary model variables are known at time  $n+1$ , and we can return to phase (A) above and start the next time step.

## 3.6 Sigma coordinates

### 3.6.1 Transformation of hydrostatic equations in $\sigma$ -coordinates

To derive the hydrostatic set of equations in  $\sigma$ -coordinates, we start with the  $p$ -coordinate version. When transforming the equations, we need to eliminate the coordinate  $p$  in (3.4.1) - (3.4.5) and replace it by  $\sigma$ . Below some elements of this transformation are presented.

#### (A) TRANSFORMATION OF DERIVATIVES

We investigate how quantities of the form  $\chi = \chi(x, y, \sigma) = \chi(x, y, p)$  behave under transformations from  $p$ - to  $\sigma$ -coordinates. For vertical derivatives we use (3.3.20) and find

$$\frac{\partial \chi}{\partial \sigma} = \frac{\partial \chi}{\partial p} \frac{\partial p}{\partial \sigma}$$

The second factor can be removed upon introducing the definition (3.3.3) of  $\sigma$

$$\frac{\partial \chi}{\partial \sigma} = \frac{\partial \chi}{\partial p} p_s \quad (3.6.1)$$

When transforming horizontal derivatives, we begin with a form of (3.3.21), i.e.

$$\left( \frac{\partial \chi}{\partial x} \right)_p = \left( \frac{\partial \chi}{\partial x} \right)_\sigma + \frac{\partial \chi}{\partial \sigma} \left( \frac{\partial \sigma}{\partial x} \right)_p$$

Using (3.3.3), the last term is expressed as

$$\left( \frac{\partial \sigma}{\partial x} \right)_p = \left( \frac{\partial}{\partial x} \right)_p \frac{p}{p_s} = - \frac{p}{p_s^2} \frac{\partial p_s}{\partial x} = - \frac{\sigma}{p_s} \frac{\partial p_s}{\partial x}$$

and

$$\left( \frac{\partial \chi}{\partial x} \right)_p = \left( \frac{\partial \chi}{\partial x} \right)_\sigma - \frac{\sigma}{p_s} \frac{\partial p_s}{\partial x} \frac{\partial \chi}{\partial \sigma}. \quad (3.6.2)$$

Transformation rules (3.6.1) and (3.6.2) are used below to transform the governing system of equations.

#### (B) TRANSFORMATION OF EQUATIONS

The *hydrostatic equation* (3.4.4) is transformed using (3.6.1) to

$$\frac{\partial \phi}{\partial \sigma} = - \frac{p_s}{\rho}.$$

Here the density  $\rho$  is usually substituted using the equation of state (3.4.1). After using (3.3.3) this yields

$$\frac{\partial \phi}{\partial \sigma} = - \frac{RT}{\sigma} \quad (3.6.3)$$

The *advection operator* in  $\sigma$ -coordinates is obtained with the help of the total differential

$$\frac{D}{Dt} = \frac{\partial}{\partial t} + u \left( \frac{\partial}{\partial x} \right)_\sigma + v \left( \frac{\partial}{\partial y} \right)_\sigma + \dot{\sigma} \frac{\partial}{\partial \sigma}, \quad (3.6.4)$$

where the vertical wind in  $\sigma$ -coordinates is given by

$$\dot{\sigma} = \frac{D\sigma}{Dt} \quad (3.6.5)$$

When transforming the *horizontal momentum equation* (3.4.5a), the transformation of the pressure gradient term  $(\partial\phi / \partial x)_p$  using (3.6.2) yields

$$\frac{Du}{Dt} - fv = - \left( \frac{\partial \phi}{\partial x} \right)_\sigma + \frac{\sigma}{p_s} \frac{\partial p_s}{\partial x} \frac{\partial \phi}{\partial \sigma} + F^x.$$

The factor  $\partial\phi / \partial\sigma$  can be replaced using the hydrostatic equation (3.6.3), whereupon

$$\frac{Du}{Dt} - fv = - \left( \frac{\partial \phi}{\partial x} \right)_\sigma - \frac{RT}{p_s} \frac{\partial p_s}{\partial x} + F^x. \quad (3.6.6)$$

The transformation of the remaining equations (3.4.1)-(3.4.5) uses the same principles (for further details see e.g. Haltiner and Williams 1980).

### 3.6.2 Summary of equations and boundary conditions

Here we summarize the governing equations in  $\sigma$ -coordinates. The coupled set of equations includes the equation of state

$$\sigma p_s = \rho RT, \quad (3.6.11)$$

the continuity equation

$$\frac{\partial p_s}{\partial t} + \nabla_\sigma \cdot (p_s \mathbf{v}) + p_s \frac{\partial \dot{\sigma}}{\partial \sigma} = 0 \quad \text{with } \mathbf{v} = (u, v), \quad (3.6.12)$$

the thermodynamic equation

$$\frac{DT}{Dt} = \frac{RT}{c_p \sigma p_s} \omega + H \quad \text{with } \omega = \sigma \left[ \frac{\partial p_s}{\partial t} + u \frac{\partial p_s}{\partial x} + v \frac{\partial p_s}{\partial y} \right] + \dot{\sigma} p_s, \quad (3.6.13)$$

the hydrostatic equation

$$\frac{\partial \phi}{\partial \sigma} = - \frac{RT}{\sigma}, \quad (3.6.14)$$

and the horizontal momentum equations

$$\frac{Du}{Dt} - fv = - \left( \frac{\partial \phi}{\partial x} \right)_\sigma - \frac{RT}{p_s} \frac{\partial p_s}{\partial x} + F^x, \quad (3.6.15a)$$

$$\frac{Dv}{Dt} + fu = - \left( \frac{\partial \phi}{\partial y} \right)_\sigma - \frac{RT}{p_s} \frac{\partial p_s}{\partial y} + F^y. \quad (3.6.15b)$$

In these equations, all "horizontal" derivatives are taken on  $\sigma$ -surfaces, and the advection operator  $D/Dt$  is given by (3.6.4).

Equation (3.6.15) exhibits a serious disadvantage of  $\sigma$ -coordinates in regions of complex topography. The horizontal pressure gradient term, which was  $(\partial\phi / \partial x)_p$  in pressure coordinates, is represented by the two terms immediately to the right of the equal sign. In cases without topography, the second term is small. However, in regions of complex topography, both the terms are much larger than the pressure gradient itself, and this often leads to substantial truncation errors. While terrain-following coordinates provide a simple strategy to map the computational domain (and for instance to represent the boundary layer), they suffer from this "pressure gradient problem". Several approaches exist to reduce these difficulties, but a general and fully satisfactory solution does not exist.

The boundary conditions (3.4.8-9) in pressure coordinates are simplified by the transition  $\sigma$ -coordinates considerably:

$$p = 0: \quad \sigma = 0 \quad \dot{\sigma} = 0 , \quad (3.6.16a)$$

$$p = p_s: \quad \sigma = 1 \quad \dot{\sigma} = 0 , \quad (3.6.16b)$$

The second conditions here guarantees that air masses cannot transit across the lower ( $p = p_s$ ) or upper ( $p = 0$ ) model boundaries.

Note that knowledge of  $u$ ,  $v$ ,  $T$  and  $p_s$  is sufficient to recover all other quantities (in particular  $\phi$  and  $\dot{\sigma}$ ). Recovering these quantities is referred to as the diagnostic step. The geopotential  $\phi$  can be gained from the vertical integration of the hydrostatic equation (3.6.14)

$$\phi(\sigma) = g z_s + \int_{\sigma}^1 \frac{RT}{\sigma'} d\sigma' , \quad (3.6.17)$$

where the integration constant was taken from lower boundary condition (3.4.7).

Recovering the vertical wind  $\dot{\sigma}$  is more complex. The vertical integration of (3.6.12) from  $\sigma' = 0$  to  $\sigma' = \sigma$  yields

$$\sigma \frac{\partial p_s}{\partial t} + \int_0^{\sigma} \nabla_{\sigma} \cdot (p_s \mathbf{v}) d\sigma' + p_s \dot{\sigma} \Big|_{\sigma} = 0 , \quad (3.6.18)$$

where we have used the upper boundary condition (3.6.16a). Solving for  $\dot{\sigma}$  yields a diagnostic relation for the vertical wind in  $\sigma$ -coordinates

$$\dot{\sigma}(\sigma) = - \frac{\sigma}{p_s} \frac{\partial p_s}{\partial t} - \frac{1}{p_s} \int_0^{\sigma} \nabla_{\sigma} \cdot (p_s \mathbf{v}) d\sigma' . \quad (3.6.19)$$

This relationship contains the surface pressure tendency  $\partial p_s / \partial t$ . It can be diagnosed by evaluating (3.6.19) at  $\sigma=1$ , i.e.

$$\frac{\partial p_s}{\partial t} = - \int_0^1 \nabla_\sigma \cdot (p_s \mathbf{v}) d\sigma . \quad (3.6.20)$$

where we have also used the lower boundary condition (3.6.16b). Equation (3.6.20) represents a prognostic equation for the surface pressure tendency as the vertically integrated mass flux divergence in the overlying atmosphere.

### 3.6.3 Numerical integration

Below we sketch a simple numerical scheme for the hydrostatic form of the governing equations in  $\sigma$ -coordinates. We assume that at time  $t$  all the quantities  $T$ ,  $u$ ,  $v$ ,  $\phi$  und  $p_s$  are known. Stepping forward in time to  $t + \Delta t$  is performed with the following steps:

- (i) Computation of surface pressure tendency  $\partial p_s / \partial t$  using (3.6.20).
- (ii) Diagnosis of vertical wind  $\dot{\sigma}$  using (3.6.19).
- (iii) Computation of tendencies  $\partial u / \partial t$ ,  $\partial v / \partial t$  and  $\partial T / \partial t$  using equations (3.6.15) and (3.6.13), respectively.
- (iv) Time step for  $u$ ,  $v$ ,  $T$  and  $p_s$  to time  $t + \Delta t$ .
- (v) Diagnosis of geopotential  $\phi$  using (3.6.17).

After these steps,  $T$ ,  $u$ ,  $v$ ,  $\phi$  and  $p_s$  are available at time  $t + \Delta t$ , whereupon the next time step may start again with (i).

For the spatial discretization, the following staggered arrangement of variables is typically used for mesoscale models (see Fig.3.6.1):

$$\begin{aligned} u: & \quad u_{i+1/2,j,k} \quad k = 1..K \\ v: & \quad v_{i,j+1/2,k} \quad k = 1..K \\ T: & \quad T_{i,j,k} \quad k = 1..K \\ \phi, \dot{\sigma}: & \quad \chi_{i,j,k+1/2} \quad k = 0..K \\ p_s & \quad p_s \quad i, j \end{aligned} \quad (3.6.21)$$

The variables  $u_k$ ,  $v_k$  and  $T_k$  are located at the center of the computational layers defined by

$$\sigma_k = (k - 1/2) \Delta \sigma \quad \text{for } k = 1..K, \quad (3.6.22a)$$

while the variables  $\phi_{k+1/2}$  and  $\dot{\sigma}_{k+1/2}$  are located at the layer interfaces defined by

$$\sigma_{k+1/2} = k \Delta \sigma \quad \text{for } k = 0..K. \quad (3.6.22b)$$

Note that the levels are numbered from top to bottom (in the sense of increasing  $p$  or  $\sigma$ ).

The vertical staggering simplifies the vertical integrations in equations (3.6.17), (3.6.19) and (3.6.20). For instance, (3.6.17) can simply be discretized as

$$\phi_{i,j,k-1/2} = g z_s + \sum_{k'=k}^K \frac{RT_{i,j,k'}}{\sigma_{k'}} \Delta\sigma = g z_s + \sum_{k'=k}^K \frac{RT_{i,j,k'}}{k'-1/2}. \quad (3.6.23)$$

The vertical staggering of the velocity components (in a similar fashion as with the shallow water equations or as in isentropic coordinates) simplifies the computation of the divergence term in (3.6.20).

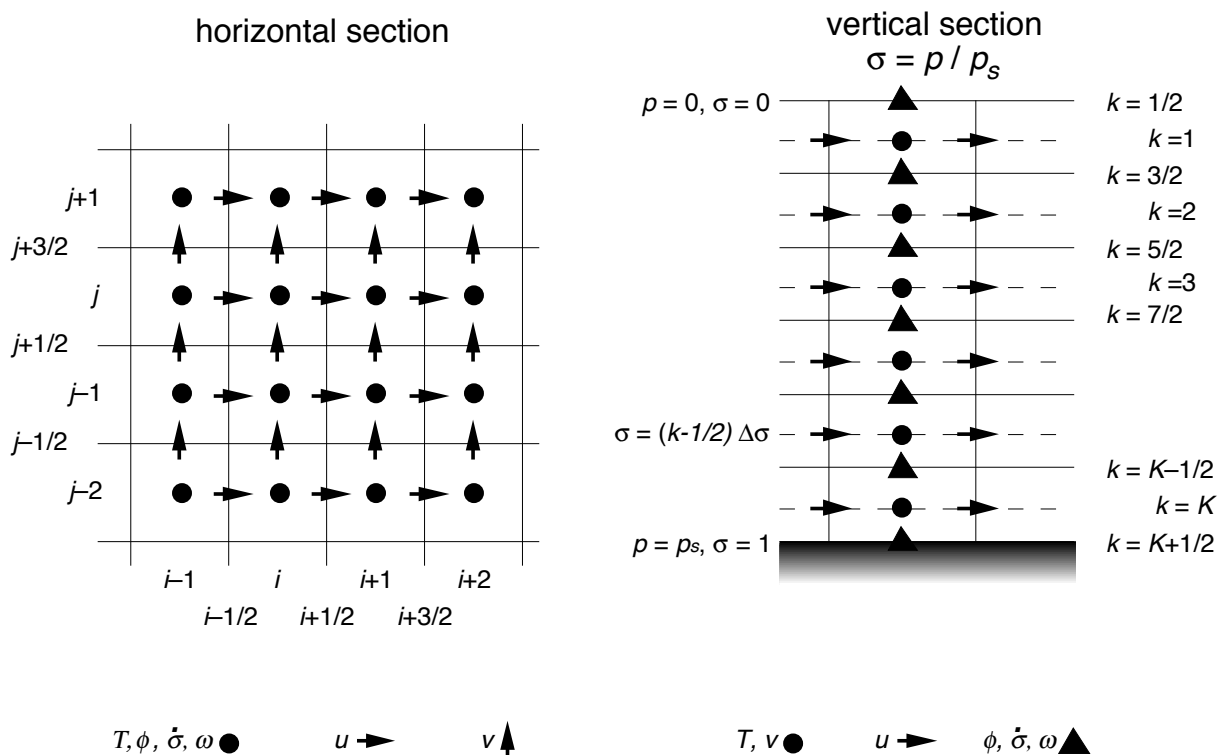


**Fig.3.6.1:** Three-dimensional distribution of variables in  $\sigma$ -coordinates.

### 3.6.4 Additional aspects of terrain-following coordinates

#### (A) HYBRID COORDINATES

Most terrain-following atmospheric models use generalized versions of the  $\sigma$ -coordinate. Of particular practical importance are hybrid approaches, which may be used to provide a smooth transition from terrain-following  $\sigma$ -type coordinates (at low levels) to pressure coordinates (at upper levels). An example of such a coordinate is shown in Fig.3.6.2. In the formulation of Simmons and Burridge (1981), the coordinates are defined by

$$p(\sigma) = a(\sigma) + p_s b(\sigma), \quad (3.6.30)$$

where the coefficients  $a$  and  $b$  represent functions of  $\sigma$ . This formulation allows a smooth transition from regions of  $\sigma$ -coordinates (characterized by  $a=0$ ,  $b=\sigma$ ) to  $p$ -coordinates (characterized by  $b=0$ ). In addition, by a clever choice of  $a$  and  $b$ , the formulation (3.6.30) allows non-equal spacings of coordinates. This is particularly useful to provide enhanced computational resolution in the boundary layer or in the troposphere (see Fig.3.6.2).

In the discretized case, (3.6.30) may be written as

$$p_{k+1/2} = a_{k+1/2} + p_s b_{k+1/2} \quad \text{for } k=0, \dots K. \quad (3.6.31)$$

Thus, the tables  $a_k$  and  $b_k$  are used to define the distribution and properties of the computational levels.

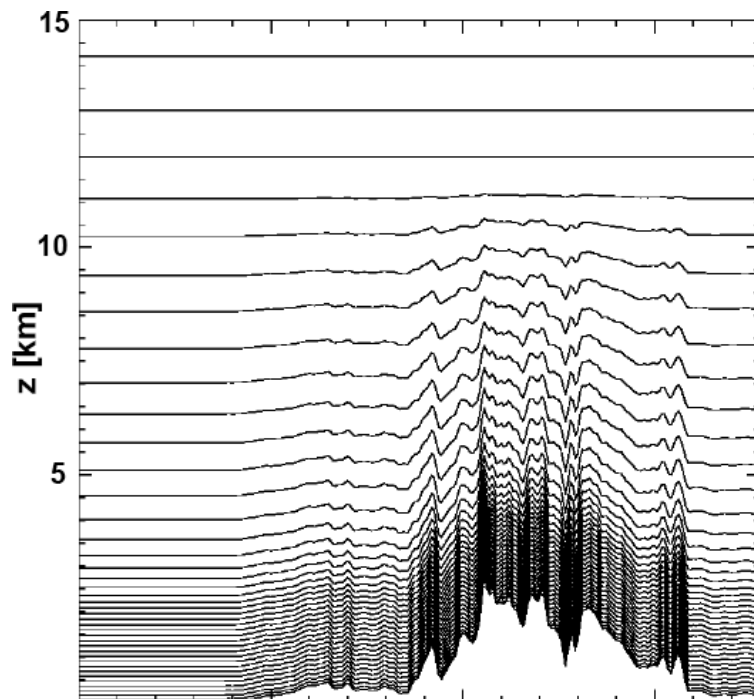


**Fig.3.6.2:** Example of computational layers in hybrid coordinates. Note the height coordinates at upper levels, and the increased resolution in the lower troposphere.

## (B) SMOOTH LEVEL COORDINATES

The use of terrain-following  $\sigma$ -coordinates implies that topographic variations appear in the coordinates at upper levels. This problem is partly but not completely alleviated by the use of hybrid coordinates (see Fig.3.6.2). The deformation of the computational mesh increases the truncation error of numerical schemes. Of particular importance are small-scale variations (that arise from small-scale topographic features), which lead to comparatively poor numerical representations, even in cases of a smooth flow.

In order to reduce this effect, smooth coordinate formulations are desirable. A simple procedure that adopts this objective is based on the use of scale-dependent coordinate formulations. More specifically, the underlying topography may be split as

$$h(x,y) = h_1(x,y) + h_2(x,y), \quad (3.6.35)$$

where the two terms  $h_1$  and  $h_2$  refer to large-scale (smooth) and small-scale (noisy) topographic contributions, respectively. The large-scale topographic contribution may be obtained by smoothing the original topography with the help of a digital filter. Smooth upper-level coordinates may then be obtained by formulations that exhibit a rapid vertical decay with height of the small-scale  $h_1$  contribution, and a slow decay with height of the large-scale  $h_2$  contribution. An example is provided in Fig.3.6.3. The net vertical displacement of the coordinate surfaces is similar in both cases, but the variations in the right-hand panel are much smoother. In comparison, the smooth coordinate considerably reduces the truncation error, in particular in cases where a smooth large-scale flow is present at upper levels. Such flows are well represented on smooth grids, but suffer considerable truncation errors on noisy grids.

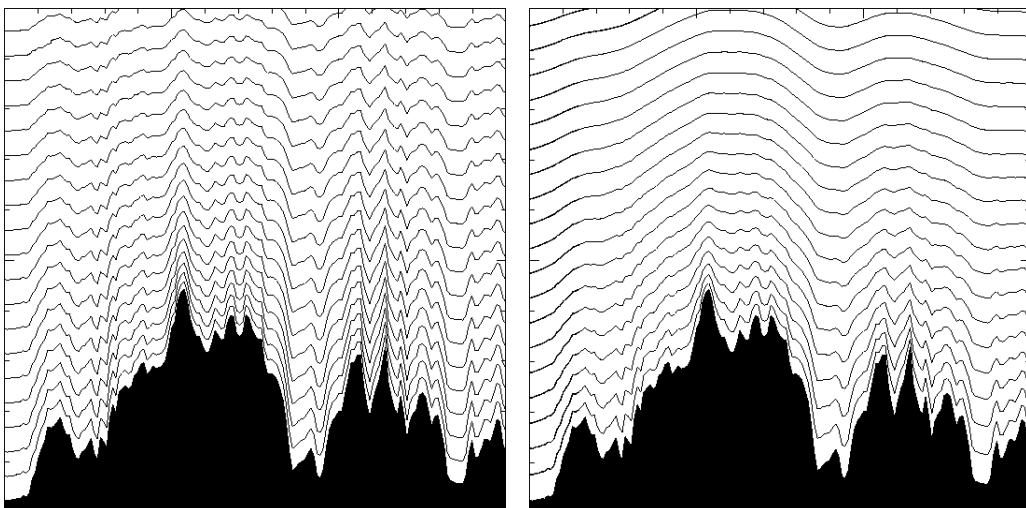


**Fig.3.6.3:** Examples of vertical coordinates in high-resolution models using (left) hybrid coordinates and (right) smooth level coordinates (Schär et al. 2002). The displayed domain encompasses the lowermost 10 kilometers, the full model domain has a depth of 25 km.

## 3.7 Spectral methods

The first step in numerical models is the discretization, which allows the representation of a continuum by a finite number of degrees of freedom. For the horizontal spatial discretization, most finite difference or finite volume approximations represent a function  $\phi(x,t)$  by grid points, usually defined as the area-average over the grid box under consideration, i.e.

$$\phi_i(t) = \frac{1}{\Delta x} \int_{x_i - \Delta x/2}^{x_i + \Delta x/2} \phi(x,t) dx . \quad (3.7.1)$$

In contrast, the spectral method expands the function  $\phi(x,t)$  using some carefully selected base functions. In simple geometries, the appropriate base functions are given by waves, thus representing  $\phi$  as a Fourier series according to

$$\phi(x,t) = \sum_m \psi_m(t) e^{ik_m x} . \quad (3.7.2)$$

The coefficients  $\psi_m$  are time dependent and describe the temporal evolution of  $\phi$ .

### 3.7.1 Classical spectral method

The Fourier expansion of  $\phi(x,t)$  in a periodic domain  $0 \leq x \leq L$  is given by

$$\phi(x,t) = \sum_{m=-M}^M \psi_m(t) \frac{1}{\sqrt{L}} e^{ik_m x} \quad \text{with} \quad k_m = m \frac{2\pi}{L} \quad (3.7.3)$$

The base functions  $L^{-1/2} e^{ik_m x}$  are orthogonal with the metric

$$\int_0^L L^{-1/2} e^{ik_m x} \overline{L^{-1/2} e^{ik_l x}} dx = \delta_{lm} , \quad (3.7.4)$$

where the overbar denotes complex conjugation. The Fourier coefficients  $\psi_m$  are complex-valued and satisfy

$$\psi_m = \overline{\psi}_{-m} \quad (3.7.5)$$

provided  $\phi$  is real-valued.

#### (A) LINEAR SYSTEMS

In the case of the linear advection equation

$$\frac{\partial \phi}{\partial t} + u \frac{\partial \phi}{\partial x} = 0 \quad (3.7.6)$$

substitution of (3.7.3) yields

$$\sum_{m=-M}^M \left[ \frac{\partial \psi_m}{\partial t} + i u k_m \psi_m \right] e^{ik_m x} = 0 . \quad (3.7.7)$$

As the base functions are orthogonal (and thus linearly independent), this equation can only be satisfied by

$$\frac{\partial \psi_m}{\partial t} = -iu k_m \psi_m \quad (m = -M \dots M) . \quad (3.7.8)$$

This corresponds to  $(2M+1)$  ordinary differential equations. For the numerical integration, we may use the Leapfrog timestep, i.e.

$$\psi_m^{n+1} = \psi_m^{n-1} - 2i\Delta t u k_m \psi_m^n . \quad (3.7.9)$$

Note that this time step (and the Asselin filter that is often used in combination with it) are complex-valued.

An important advantage of the spectral method is the fact that the spatial discretization (3.7.8) is error free. The truncation error in (3.7.9) is exclusively due to the temporal discretization. Analysis using the Von Neumann method (with  $\psi_m^{n+1} = \lambda \psi_m^n$ ) yields

$$\lambda_{1,2} = -i p \pm \sqrt{1 - p^2} \quad \text{with} \quad p = u \Delta t k_m . \quad (3.7.10)$$

The linear advection with the spectral scheme is thus stable and neutral ( $|\lambda| = 1$ ) for

$$|\Delta t u k_m| \leq 1 . \quad (3.7.11)$$

This condition can be interpreted as a modified form of the CFL criterion (instead of  $\Delta x$ , the horizontal length scale is given by  $1/k$ ). A comparison between the spectral method (using the Leapfrog time step) and centered finite differencing is shown in Fig.3.7.1 (where it was assumed that  $|k_M| = \pi/\Delta x$ ). It illustrates that the phase error of the spectral method is considerably smaller for most relevant wave numbers. For  $\alpha=0.5$ , for instance, the phase error

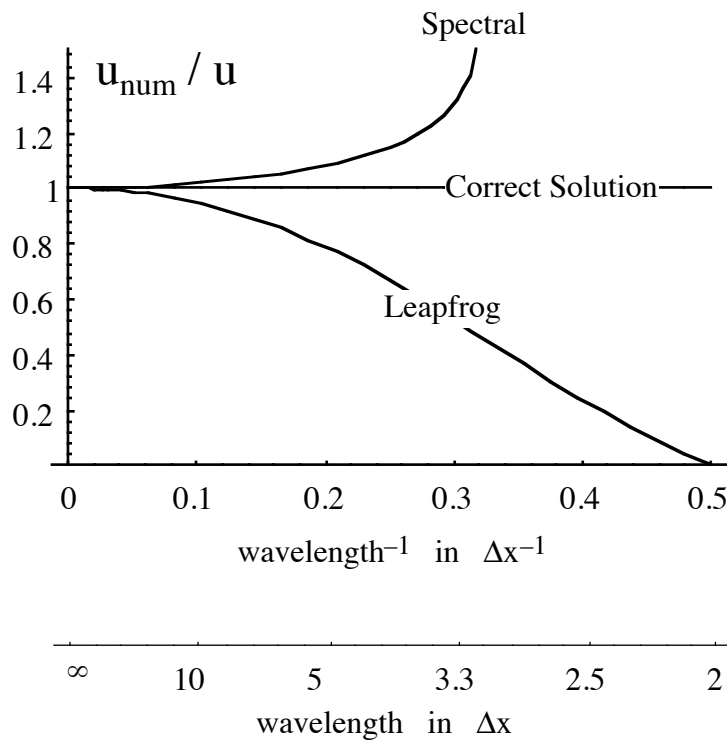


**Fig.3.7.1:** Phase error of the spectral method for the linear advection equation with Courant number  $\alpha=0.5$ , in comparison with centered differencing.

of  $4\Delta x$  waves is only half as large as the corresponding error for centered differencing. Thus, spectral models can run at lower spatial resolution and are still competitive with centered finite difference schemes. However, the stability criterion (3.7.11) is slightly more restrictive.

## (B) NONLINEAR SYSTEMS

In the nonlinear case

$$\frac{\partial u}{\partial t} + u \frac{\partial u}{\partial x} = 0 \quad (3.7.12)$$

some of the advantages of the spectral methods disappear. In particular, using a representation like (3.7.3) for  $u$ , and introducing it into (3.7.12) yields

$$\frac{1}{\sqrt{L}} \sum_{m=-M}^M \frac{\partial \psi_m}{\partial t} e^{ik_m x} + \frac{1}{L} \left[ \sum_{j=-M}^M \psi_j e^{ik_j x} \right] \left[ \sum_{l=-M}^M i k_l \psi_l e^{ik_l x} \right] = 0$$

or

$$\frac{1}{\sqrt{L}} \sum_{m=-M}^M \frac{\partial \psi_m}{\partial t} e^{ik_m x} + \frac{1}{L} \sum_{j,l=-M}^M \psi_j i k_l \psi_l e^{ik_{j+l} x} = 0, \quad (3.7.13)$$

where  $k_{j+l} = k_j + k_l$ . The second sum of the latter equation has  $(2M+1)^2$  terms. To derive an equation for the individual coefficients, (3.7.13) is multiplied by the complex conjugated base function, i.e.  $L^{-1/2} e^{-ik_p x}$ , and integrated over the computational domain  $0 \leq x \leq L$ . Using (3.7.4), this yields

$$\frac{\partial \psi_p}{\partial t} + \frac{1}{L} \sum_{j,l=-M}^M \psi_j \psi_l \int_0^L i k_l e^{ik_{j+l-p} x} dx = 0 \quad (p = -M \dots M).$$

This can be represented as

$$\frac{\partial \psi_p}{\partial t} = - \sum_{j,l=-M}^M I_{j,l,p} \psi_j \psi_l \quad (p = -M \dots M), \quad (3.7.14a)$$

where

$$I_{j,l,p} = \frac{1}{L} \int_0^L i k_l e^{ik_{j+l-p} x} dx. \quad (3.7.14b)$$

denote the *interaction coefficients*. In our special case of the advection equation (3.7.12), the interaction coefficients  $I$  can easily be computed as

$$I_{j,l,p} = i k_l \delta_{j+l,p}. \quad (3.7.15)$$

In more general cases, the evaluation of  $I$  will be costly, and one would ideally like to compute  $I$  once (before beginning the integration) and store the result. This requires, however, a gigantic amount of memory as the matrix  $I$  has  $(2M+1)^3$  elements. For complex models (such as spectral NWP and climate models),  $M$  may be of the order  $10^5$  (for each variable and

level), which would require huge memory (in the order of several Petabytes). Hence the spectral approach in its basic form is not feasible.

On the other hand the nonlinear spectral approach has an important advantage. It suppresses the Aliasing error (and nonlinear instability, see Schär 2006, chapter 5). More specifically, consider the generation (by nonlinear interactions) of a wave  $e^{ik_{j+l}x}$  that cannot be represented by the base functions considered (i.e.  $|j+l| > M$ ). According to (3.7.14), such a wave will not affect the results. Thus, the spectral method does not suffer from the type of nonlinear instability problems that are common with finite difference approaches.

### 3.7.2 Pseudo-spectral method

The pseudo-spectral method exploits the advantages of the spectral approach (high accuracy, absence of nonlinear instability) but avoids its key disadvantage (limited applicability to nonlinear problems). In essence, the spectral space computations are restricted to linear operations, while the nonlinear operations are evaluated in physical space on a regular grid

$$x_i = i \Delta x \quad (1 \leq i \leq N) \quad (3.7.20)$$

The switch between the two discretizations is accomplished using Fourier transforms (FT).

In the case of the non-linear advection equation (3.7.12), a single time steps implies the following operations:

(i) Computation of derivative  $\partial u / \partial x$  in spectral space as  $i k_l \psi_l$ .

(ii) Transformation of  $u$  and  $\partial u / \partial x$  from spectral to physical space:

$$FT^{-1} : \psi_l^n \rightarrow u_i^n$$

$$FT^{-1} : i k_l \psi_l^n \rightarrow \left( \frac{\partial u}{\partial x} \right)_i^n$$

(iii) Computation of tendency in physical space:

$$\left( \frac{\partial u}{\partial t} \right)_i^n = -u_i^n \left( \frac{\partial u}{\partial x} \right)_i^n$$

(iv) Transformation of tendencies back to spectral space:

$$FT: \left( \frac{\partial u}{\partial t} \right)_i^n = \sum \tilde{\psi}_m^n e^{i k_m x} \rightarrow \tilde{\psi}_m^n .$$

(v) Time step (e.g. using the Leapfrog scheme) in spectral space:

$$\psi_m^{n+1} = \psi_m^{n-1} + 2 \Delta t \tilde{\psi}_m^n .$$

In this way, there is no need to store the interaction coefficients. As the spatial derivatives are computed in spectral space, the pseudo-spectral method has small truncation errors.

Some further considerations are needed regarding the choice of the resolutions in spectral and physical space. The simplest approach defines the physical grid using

$$N = 2 M \quad (3.7.21)$$

grid points within the periodic domain. With this choice, standard Fourier transform techniques may be used. However, with (3.7.21) the pseudo-spectral method is not Aliasing-free. For quadratic nonlinear interactions, such as in (3.7.12), aliasing-free results are obtained with the alternative choice

$$N = 4 M. \quad (3.7.22)$$

With this choice, the resolution in physical space is twice that of the resolution in computational space, and all quadratic interactions can be properly represented in step (iii). When transforming the tendencies back to physical space in step (iv), the fine-scale contribution of the tendencies is automatically filtered, and is thus unable to contaminate the spectrum and induce nonlinear instability as in finite difference implementations.

The pseudo-spectral method has only become attractive in the late 1960s, after the discovery of the Fast Fourier Transform (FFT) by Cooley and Tukey in 1965. Their algorithm dramatically reduced the computational requirements of Fourier transforms. Evaluating the Fourier transform directly would take  $O(N^2)$  arithmetical operations, while with FFT the same result can be obtained in only  $O(N \log N)$  operations. Prior to the discovery of the FFT, the pseudo-spectral method was computationally too expensive for realistic atmospheric applications.

### 3.7.3 Global spectral models

Pseudo-spectral methods are very popular in global atmospheric weather and climate models. Beyond the advantages listed above, there is one important additional motivation: Grid point methods using a regular grid in spherical coordinates  $(\lambda, \varphi)$  suffer from the “pole problem.” The pole is a singularity of the mapping from the sphere to the  $(\lambda, \varphi)$ -plane. There is no simple solution to this problem, as all sphere-to-plane mappings have singularities.

The spectral approach on the sphere is an elegant solution to the pole problem, and it is the only numerical method that represents a sphere completely isotropically. The spectral base functions on the sphere are the spherical harmonics  $Y_n^m(\lambda, \varphi)$ . These are defined as the eigenfunctions of the Laplace operator, i.e.

$$\nabla^2 Y_n^m = -\frac{n(n+1)}{a^2} Y_n^m \quad \text{for } |m| \leq n. \quad (3.7.25)$$

Here  $m$  and  $n$  are referred to as the *order* and *degree* of  $Y_n^m(\lambda, \varphi)$ , respectively, and  $a$  denotes the Earth's radius. The spherical harmonics can be considered a generalization of plane waves on the sphere. They can be expressed as

$$Y_n^m(\lambda, \varphi) = P_n^m[\sin(\varphi)] e^{im\lambda} . \quad (3.7.26)$$

where  $P_n^m$  denote the associated Legendre polynomials of order  $m$  and degree  $n$ . The order  $m$  determines the variations in the direction of  $\lambda$  (longitude), and spherical harmonics of the  $Y^m$  family have a zonal wave number  $m$  (i.e.  $m$  waves in West-East direction along a latitude circle). The variations in the direction of  $\varphi$  (latitude) are more complex and described by the Legendre polynomials. Selected examples of spherical harmonics are shown in Fig.3.7.2.

In the global spectral approach, all two-dimensional fields are expanded into series of spherical harmonics of the form

$$\phi(\lambda, \varphi, t) = \sum_{m=-M}^M \sum_{n=|M|}^{N(m)} \psi_n^m(t) Y_n^m(\lambda, \varphi) . \quad (3.7.27)$$

There are two standards for the truncation of the series, i.e. how to choose  $M$  and  $N(m)$ . These are referred to as *triangular* and *rhomboidal* truncation, respectively (see Fig.3.7.3 for  $M=4$ ). As example, consider the global deterministic weather forecasting model of the European Centre for Medium-Range Weather Forecasts (ECMWF). It is currently based on the triangular truncation “T799.” Here “T” refers to triangular, and “799” denotes the truncation of the zonal wave number at  $M=799$ . The smallest represented wave in this truncation has a wave length of  $40,000 \text{ km} / 799 = 50 \text{ km}$ . This corresponds to a grid-point resolution of about

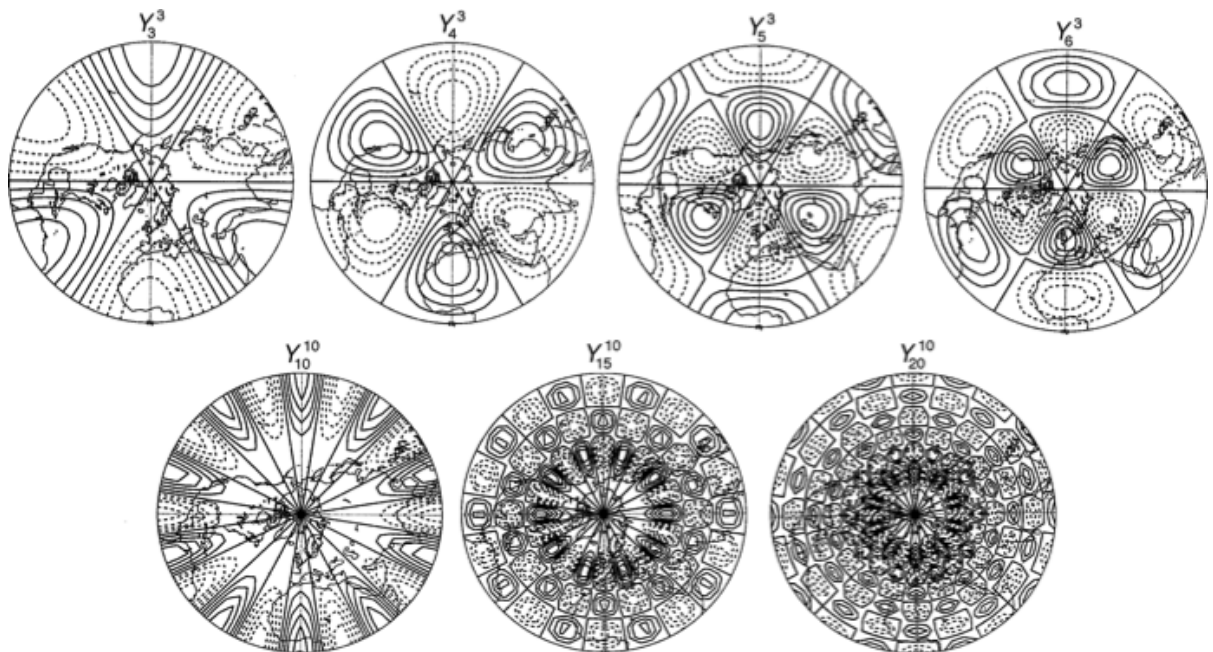


**Fig.3.7.2:** Examples of spherical harmonics. Upper and lower panels show members of the families  $Y_x^3$  und  $Y_x^{10}$  with zonal wave numbers 3 and 10, respectively.

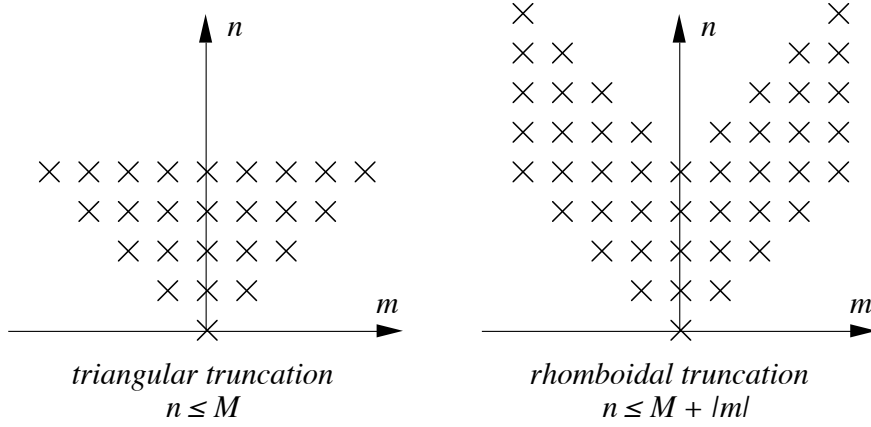


**Fig.3.7.3:** Triangular and rhomboidal truncation of spherical harmonics for  $M=4$ .

25 km (assuming 2 grid points per wave length).

Global spectral models exploit a series of relationships that directly derive from the properties of the spherical harmonics. In particular, many elementary operations become simplified in spectral space. For instance, the computation of spatial derivatives is computationally very simple (see Riddaway and Hortal 2001)

$$\frac{\partial}{\partial \lambda} Y_n^m = i m Y_n^m \quad (3.7.28a)$$

$$\frac{\partial}{\partial \varphi} Y_n^m = -n \varepsilon_{n+1}^m Y_{n+1}^m + (n+1) \varepsilon_n^m Y_{n-1}^m \quad \text{with} \quad \varepsilon_n^m = \sqrt{\frac{n^2 - |m|^2}{4n^2 - 1}} \quad (3.7.28b)$$

while the mathematics behind these relations is rather cumbersome.

It is important to realize that the computational requirements of the spectral method grow rapidly with increasing resolution, much faster than the number of grid points involved, even when using Fast Fourier Transforms (FFT). For illustration, consider a two-dimensional regular grid in flat geometry with  $N \times N$  gridpoints. In a finite difference model, the computational requirements per time step will increase with the number of gridpoints as  $N^2$ . In a spectral model it will increase with  $N^2 \log_2(N)$ , as a two-dimensional transform implies  $2N$  one-dimensional transforms of length  $N$ , and as a one-dimensional FFT requires  $N \log_2(N)$  operations. These relations suggest that at some time in the future, gridpoint models will become computationally advantageous. Thus, there is currently a thrust towards developing high-resolution global models using sophisticated grids (such as spherical cube or geodesic grids).

### 3.8 References

- Davies, T., 2002: *Adiabatic formulation of models*. Lecture Series, Meteorological Training Course. ECMWF, 33pp,  
[http://www.ecmwf.int/newsevents/training/lecture\\_notes/pdf\\_files/NUMERIC/Adiabat.pdf](http://www.ecmwf.int/newsevents/training/lecture_notes/pdf_files/NUMERIC/Adiabat.pdf)
- Durran, D.R., 1998. *Numerical Methods for Wave Equations in Geophysical Fluid Dynamics*. Texts in Applied Mathematics **32**, Springer, New York, 465pp
- Fletcher, C.A.J, 1991: *Computational Techniques for Fluid Dynamics*. Vol. 1 and 2., second edition, Springer, Berlin, 401pp and 493pp
- Gal-Chen, T. and R. Sommerville, 1975: On the use of a coordinate transformation for the solution of the Navier-Stokes equations. *J. Comp. Phys.*, **17**, 209-228
- Gill, A., 1982. *Atmosphere-Ocean Dynamics*. Academic Press, 662pp
- Haltiner, G.J. and R.T. Williams, 1980. *Numerical prediction and dynamic meteorology*. John Wiley & Sons, New York, 477pp
- Holton, J. R., 2004: *An introduction to dynamic meteorology*. 4th edition. Academic Press / Elsevier, New York, 530pp
- Kalnay, E., 2003: *Atmospheric Modeling, Data Assimilation and Predictability*. Cambridge University Press, Cambridge UK, 341 pp
- Landau, R.H. and M.J. Páez, 1§997. *Computational Physics. Problem Solving with Computers*. Wiley, New York, 520pp
- Pielke, R.A. 1984: *Mesoscale meteorological modelling*. Academic Press, New York, 612pp
- Press, W.H., B.P. Flannery, S.A. Teukolsky, W.T. Vetterling, 1989. *Numerical Recipes: The Art of Scientific Computing*. Cambridge University Press, Cambridge, 702
- Riddaway, R.W. and M. Hortal, 2001. *Numerical Methods*. Lecture Series, Meteorological Training Course. ECMWF. 98pp,  
[http://www.ecmwf.int/newsevents/training/lecture\\_notes/pdf\\_files/NUMERIC/Num\\_meth.pdf](http://www.ecmwf.int/newsevents/training/lecture_notes/pdf_files/NUMERIC/Num_meth.pdf)
- Schär, C., D. Leuenberger, O. Fuhrer, D. Lüthi and C. Girard, 2002: A new terrain-following vertical coordinate formulation for atmospheric prediction models. *Mon. Wea. Rev.*, **130**, 2459-2480
- Schär, C., 2006: *Numerische Methoden in der Umweltphysik*, lecture notes ETH Zürich,  
<http://www.iac.ethz.ch/staff/schaer/Vorlesungen/NumUmwelt/>
- Simmons, A. J. and D. M. Burridge, 1981: An energy and angular-momentum conserving finite-difference scheme and hybrid vertical coordinates. *Mon. Wea. Rev.*, **109**, 758-766
- Simmons, A.J., 1994: Adiabatic formulation of large-scale models of the atmosphere: Finite-difference schemes for the horizontal discretization. Lecture Series, Meteorological Training Course. ECMWF, 16pp,  
[http://www.ecmwf.int/newsevents/training/lecture\\_notes/pdf\\_files/NUMERIC/Dscretiz.pdf](http://www.ecmwf.int/newsevents/training/lecture_notes/pdf_files/NUMERIC/Dscretiz.pdf)

Zhu, Z., J. Thuburn, B.J. Hoskins and P.H. Haynes, 1992: A vertical finite-difference scheme based on a hybrid sigma-theta-pressure coordinate. *Mon. Wea. Rev.*, **120**, 851-862